Delft University of Technology

Thesis

Soil-grout interface friction for HDD installed heat transport pipes

Author:
Lodewijk Pleij (4333217)

August 24, 2022

Contents

1 Introduction **3**

2 Literature study **6**
2.1 Horizontal Directional Drilling . . . 6
2.1.1 Borehole stability in HDD . . . 6
2.1.2 Borehole pressure . . . 6
2.2 Drilling fluids . . . 8
2.2.1 Mineralogy . . . 8
2.2.2 Thixotropy . . . 9
2.2.3 Building material . . . 10
2.2.4 Filter cake . . . 10
2.3 Drill-grout . . . 11
2.4 Medium pipe . . . 13
2.5 Friction . . . 13
2.5.1 Roughness . . . 13
2.5.2 Micro-scale roughness . . . 14
2.5.3 Macro-scale roughness . . . 14
2.6 Bentonite and drill-grout intrusion . . . 14
2.6.1 Borehole pressure . . . 14
2.6.2 Soil infiltration . . . 15

3 Test methods **17**
3.1 Shear test . . . 17
3.2 Dynamic pipe interaction method . . . 18
3.2.1 How the DPIA is built . . . 18
3.3 Sample preparation . . . 20
3.3.1 Direct shear test . . . 20
3.3.2 DPIM . . . 21
3.4 Methodology . . . 21
3.4.1 Shear test . . . 21
3.4.2 DPIM . . . 21

4 Results **23**
4.1 Direct shear test . . . 23
4.2 Dynamic pipe interaction method . . . 23
4.2.1 Observations . . . 23
4.2.2 Explanation graphs . . . 24
4.2.3 Polynomial fit . . . 26
4.2.4 Normalisation . . . 27
4.2.5 Correction for the friction of the system . . . 29
4.2.6 Test 1, 2 and 4 . . . 30

5 Calculations **33**
5.1 Grout to soil interface friction calculation . . . 33
5.2 Design of heat transportation lines . . . 35
5.2.1 Friction factor comparison . . . 35
5.2.2 Normal force due to pressure build up . . . 36

6 Conclusion **37**

7 Experience and recommendations **38**
7.1 Experience . . . 38
7.2 Recommendations . . . 41

Abstract

The soil-grout interface friction was measured to be in between 0.0 [kPa] and 14 [kPa]. To measure this friction, a special research method was invented that enabled a tunnel to be recreated. With this setup, any formation could be used. The formation could be created with a hole in the middle which simulated a borehole. Next, by filling and pressurising this hole with a bentonite-water suspension, a stable borehole could be simulated. This borehole was then filled with drillgrout to recreate a tunnel filled with grout. This grout column could then be pulled out of the soil formation so that the friction between the drillgrout and soil could be measured. In this setup, no normal forces were present. Due to the absence of normal forces no friction angle could be deducted which made it impossible to estimate the effect of the friction at the depth where a pipe laid by HDD would generally be found. It was concluded that based on the data found, it is not recommended to use grout as a borehole filling around heat transportation pipes. Although the friction would be mainly determined by the filter cake strength, which is comparable to a weak clay, effects like irregular borehole diameters and large soil stresses at the depth of the pipe, would create a frictional force that is large enough to cause buckling or failure of the insulating PUR layer.

1 Introduction

With pollution levels and energy prices rising, energy efficiency is becoming more and more important. One of the sectors that has still a lot to gain considering energy efficiency is the industrial sector. One of the many ways to increase the energy efficiency of the industrial sector is by reusing unused heat that is created by factories or power plants. Normally, heat is used or created as a by-product to create the product that is being produced by the factories. This heat is then considered as waste and emitted through water or into the air. One of the ways to increase the energy efficiency of these factories is to reuse the heat to warm houses. The heat is being stored into water or another heat bearing fluid, and transported to the desired location through heat transportation pipes. Because of logistical advantages and thermal isolation, these pipes lie almost always underground. Because the temperature of the medium that is transported trough the pipe fluctuates, the length of the pipe will expand and contract over time. To make sure that the pipe is able to expand, expansion loops are constructed 1. These loops are directed orthogonal from the main direction of the pipe. Because of the loops, the pipeline has room to expand along its length axis. Without these loops, the stresses in the pipe could build up to such a level that the material could fail.

Figure 1: An example of an expansion loop (photo credit: VHM Solutions Pty LTD)

To construct one of these "heat transportation pipelines" or any other underground pipeline, two options exist: Open trench method and trenchless method. In the open trench method, a trench will be dug out so that the pipe can be constructed. When the construction of the pipe is completed the trench can be closed with the excavated soil. In many cases, this method is the most economical and therefore used the most. But nowadays, there are more and more reasons to choose for trenchless which increases its popularity. One of them is safety. In the US alone more than 30 construction workers are killed each year nationwide in trenching or excavation-related incidents and many more obtain injuries[2]. Another downside of open trench works is the disruption of traffic and rivers. Luckily, threnchless technologies are developing faster than ever causing their costs and risks to decrease significantly.

A well known trenchless technology is horizontal directional drilling (HDD). This method starts with a so called pilot hole that is launched at a 8-16° angle[26] from surface level. After the pilot hole is constructed, it will subsequently be enlarged with a reamer. After this, the medium pipe can be pulled in place. To maintain borehole stability and transport the soil out of the borehole all throughout these steps, a drilling fluid is used which, in most cases, is a bentonite suspension.
Because the borehole is always larger than the installed pipe, there is a void in between the soil and the pipe that will be filled with the drilling fluid. Due to its thixotropic properties, bentonite slurry solidifies when it is in static state. This should create a sealed and stable borehole. Only the problem is that bentonite slurry is thixotropic. Once The maximum shear stress of the slurry is reached, the effective shear stress of the bentonite slurry will reduce to virtually zero, which causes it to become fluid again. Any aquifer with a hydraulic head higher than ground level exerts a certain stress on the bentonite slurry which causes a risk of seepage. This,

along with other reasons like long term borehole stability has caused the Dutch water management agency to have strict environmental laws that require companies, in many cases, to fill the borehole such that no seepage and settlement could occur [6].

One of the solutions to stabilise the borehole is to replace the bentonite in the borehole with grout. The grout used for this process is a mixture of relatively weaker cement types and bentonite. The bentonite is added to create a higher viscosity. This mixture is also referred to as dammer or drill-grout. Please note that different types of drill-grout are used for different projects. Also, the composition of specific drill-grout mixtures are sometimes adjusted during the project. Although drill-grout is the least desirable material for sealing and backfilling the borehole[11] considering workability, it is accepted for offering long term stability to the borehole. The permeability of drill-grout is just like cement virtually impermeable. The permeability of the drill-grout used in this research is 10^{-9} m/s[5], which is comparable to an average clay[22]. The shear strength of drill-grout after 28 days is in the order of 22kPa [5] which makes it much stronger than bentonite. Due to this it is expected that the friction between drill-grout and soil will be higher and the pipe will experience a higher resistance when the borehole is filled with drill-grout.
For most heat transportation pipes, a steel-polypurethaan(PUR)-polyetheen(PE) medium pipe is used. These are pre-insulated pipe systems where the inner transport medium is connected with a PUR layer to the protecting outer pipe. Although multiple materials are available, generally the inner transport medium is made from steel, the isolation layer is made from PUR and the outer protecting layer is made from PE[24]. When hot water is transported through the pipe, the steel pipe will expand. PUR, which has a shear strength of 40 kPa[16], is able to exert such a tensional force on the outer PE pipe that it is able to expand with the inner metal pipe (see figure 2).

Because of the shear thinning properties of bentonite, its shear strength is regarded to as 0 in the design phase. Because the shear strength is 0, there is no effective friction between the bentonite slurry and the soil and pipe. Drill-grout however, does have a shear strength that could cause a significant friction with both the soil and the pipe. Due to this, the expansion of the outer HD-PE pipe may be hindered when it is covered in grout. Another effect caused by this, is that the tension on the PUR may become higher than what is accounted for. It is key to know what the friction angle between drill-grout to soil is, so that the effects of the expansion of the pipe can be predicted effectively.

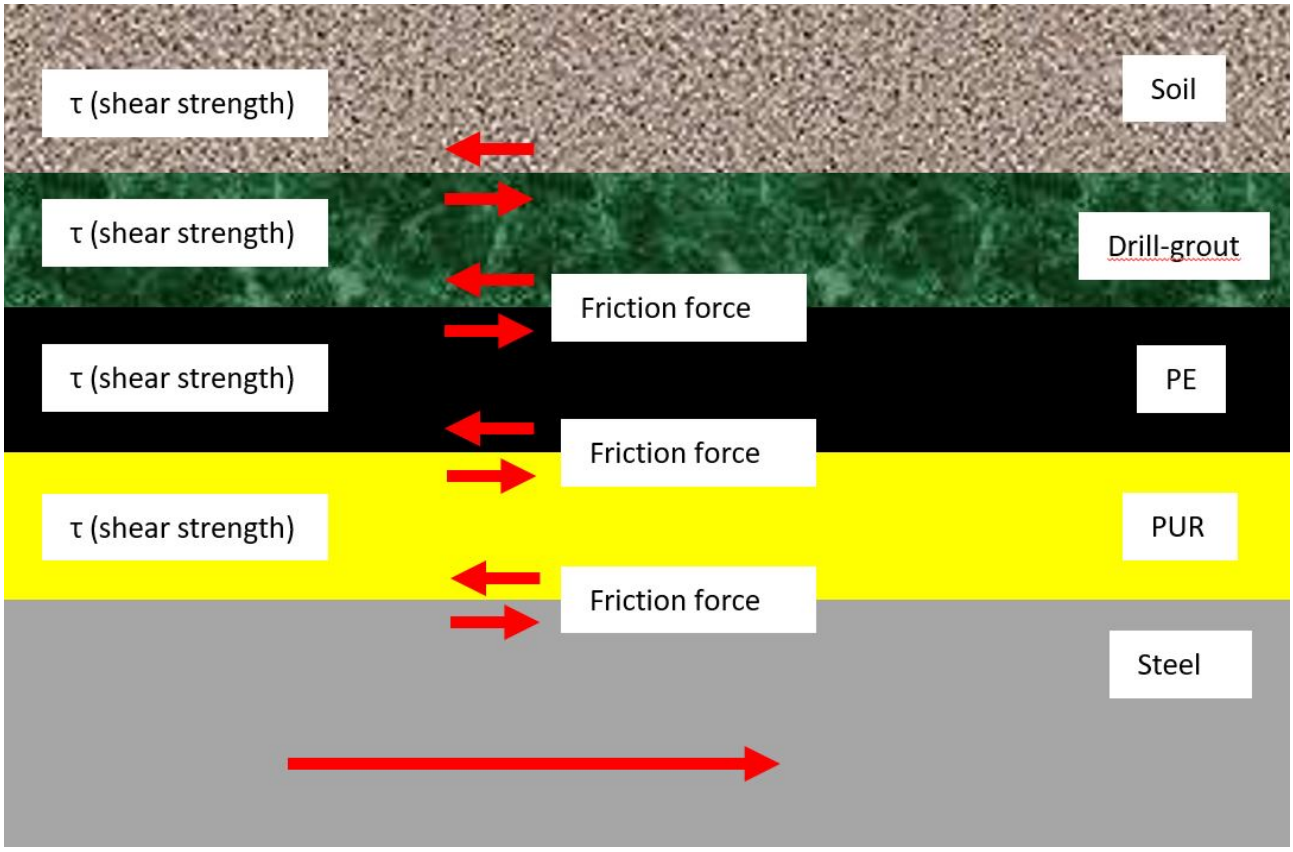

Figure 2: Longitudinal cross section of a steel-PUR-PE pipe in the soil with grout

Research questions:

What is the maximal shear stress that can occur between drill-grout and soil?

Is there a need to account for the friction between drill-grout and soil in the design of any pipe lain by HDD?

To answer these questions, tests will be done to measure the friction between the drill-grout an the soil. These tests will be done in the laboratory with one specific type of drill-grout and one specific soil type. A new research method will be developed which will enable the researcher to create a small scale tunnel with an arbitrary drilling fluid, soil and drill-grout. Then, this drill grout can be pulled out of the soil to find the friction.

First, the report will start with a literature research in which everything there is to find about drilling fluids and drill-grout will be discussed. After this, the methodology and results are discussed. After the conclusion there will be an elaborate discussion about the experience enhanced with the research method and material used.

2 Literature study

2.1 Horizontal Directional Drilling

Trenchless techologies describe all construction methods that do not require digging open trenches for the construction of underground pipes. The mostly used trenchless technologies are: Horizontal Direction Drilling (HDD); Microtunneling (MTM); Pipe Ramming (PR) and Pipe Jacking (PJ).
PJ and PR are relatively straight forward techniques since they rely on the principle of pushing the pipe through the soil from point A to B. HDD and MTM however, are techniques that are in need of relatively advanced equipment and thus, are relatively new and expensive. For MTM there is a need of a tunnel boring machine (TBM) which makes it a relatively expensive technique. Although HDD is comparatively a bit less expensive, factors like the length and borehole instability are its main disadvantages.

Horizontal directional drilling (HDD) is a method that has its roots in the oil and gas industry. HDD starts with the launch of the so called pilot hole. The pilot hole is launched by a drill rig from surface level at a 8-16 degree angle [26]. After it reaches the desired depth it will continue horizontally until it is steered upwards towards the surface. After the pilot hole is completed the hole will be enlarged to the required diameter with a reamer. When the hole is large enough, the pipe will be pulled in and the project is completed. Meanwhile, to maintain borehole stability and transport the excavated soil, a drilling fluid is used. This is an oversimplified example and note worthy exceptions will be discussed further in this chapter.

2.1.1 Borehole stability in HDD

In any soil underneath the subsurface, normal stresses and shear stresses will be present. Generally, the stress parameters used to describe the stress state of the soil are effective vertical stress σ', total vertical stress σ and pore water pressure p. The effective stress is equal to the total stress minus the pore water pressure. This results in the following formula: $\sigma' = \sigma - p$. When the pore water pressure is equal to the total stress (thus $\sigma' = 0$) liquefaction occurs.
In the case of a borehole, soil is excavated underground. This causes a drop of total stress in the soil surrounding the borehole. Due to the distribution of stresses, the soil on the side of the borehole is able to sustain itself. But, at the top of the borehole, there will be no external forces that prevent the soil from falling down. Only the cohesion of the soil can keep the borehole stable. Also, when water flows into the borehole, the soil could erode.

There are two mechanisms that will generally initiate a soil collapse. When the effective stress reduces to 0 combined with the flow of water which causes erosion. The first will only occur at the top side of the borehole while the second could occur all around the borehole. To prevent these events from happening and to export the excavated soil, a drilling fluid is used. The fluid is pumped into the borehole with a high enough pressure to prevent groundwater flow into the borehole. This fluid is almost always a mixture of bentonite and water which is called "bentonite slurry". The reason why bentonite slurry is used is because it provides a yield stress that makes it possible for soil particles to be suspended in the drilling fluid. Also, the bentonite will react mechanically, chemically and thermally with the water and surrounding soil. A so called "filter cake" will form on the borehole wall which provides a low permeability layer and extra borehole stability[23].

2.1.2 Borehole pressure

The fluid pressure in the borehole must be sufficient to prevent soil collapse and it must not be too high to prevent a blow out. The minimal required borehole pressure is dependent on the borehole length, borehole radius, drill bit radius, bore fluid parameters and the soil parameters along the borehole. The minimum borehole pressure is the required pressure to maintain borehole stability while providing the transportation of the soil towards the surface. Here, the required pressure for the transportation of the soil is higher than the pressure required to maintain borehole stability. The maximum allowable pressure is dependent on the radius and depth of the borehole and the resistance of the soil. During the pilot phase the borehole pressure is always the highest because of the required flow for the transportation of cuttings, back to the entry hole. After the pilot phase comes the reaming phase and during this phase the borehole radius increases and the drilling fluid can now flow in two directions. So, in most cases it can be assumed that the maximum amount of borehole pressure and thus the highest change of a blow-out (minimal required borehole pressure exceeding the maximal

allowable borehole pressure) is reached at the end of the pilot hole[14].This is only logical since the borehole is relatively small and the path for the transportation of cuttings is the longest. This requires a high fluid pressure.

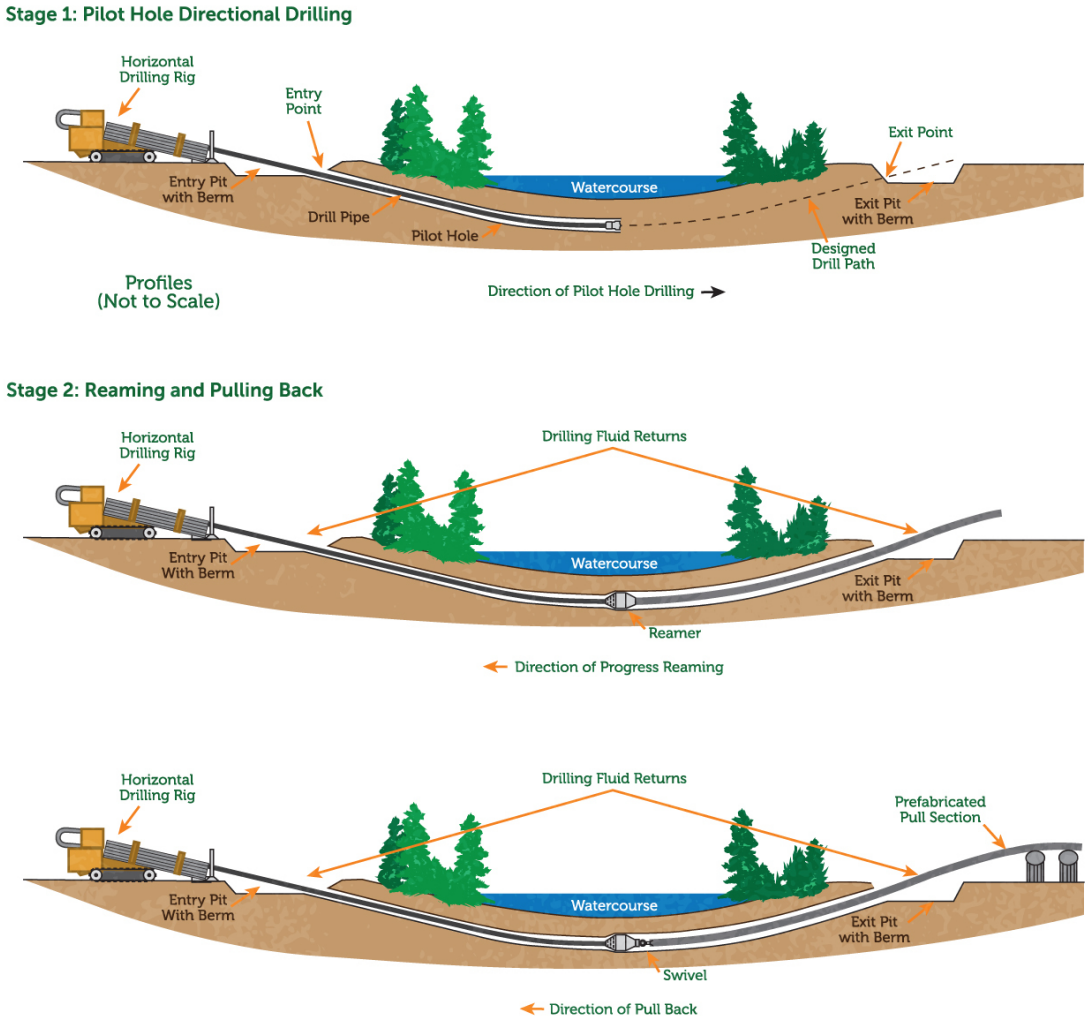

Figure 3: A 2D representation of an arbitrary HDD project. (Photo credit: https://www.transmountain.com/news/2019/digging-deeper-trenchless-crossing-methods-reduce-impact)

When a borehole collapse occurs, there is failure of the soil structure surrounding the borehole. This leads to material falling into the borehole. This generally happens when the borehole pressure is lower than the surrounding pore pressure of the soil.

According to NEN-3650-1 (latest version 2020) the following formula can be used to calculate the maximum allowable mud pressure:

$$p_{max} = (p'_f + c * cot\varphi)(R_o/R_{p,max})^2 + Q)^{\frac{-sin\varphi}{1+sin\varphi}} - c * cot\varphi + u \tag{1}$$

Where:
p_{max} is the maximum allowable mud pressure, in N/mm^2;
p'_f is the effective drill fluid pressure where the first plastic deformations will occur in N/mm^2 $p'_f = \sigma'_o * (1 + sin\varphi) + c * cos\varphi$;
σ'_o is the initial effective stress (terrainstress), in N/mm^2;
φ is the internal friction angle, in degrees;

c is the cohesion, in N/mm^2;
R_o is the initial radius of the borehole, in mm;
Q is $(\sigma'_o * sin\varphi + c * cos\varphi)/G)$;
G is the shear modulus, in N/mm^2;
$R_{p,max}$ is the maximum allowable radius of the plastic zone, in mm;
u is the pore pressure in the specific layer;
H is the height of the soil cover from the subsurface to the centre of the borehole;

Using equation 1, the borehole pressure can be calculated for different hypothetical scenarios. After injecting the drill-grout, the drill-grout will be subjected to its own static pressure. This means that the drill-grout pressure in the borehole is dependent on the depth of the borehole and can be calculated with the following formula: $p = g*D*V$, where g is the gravity constant $9.81m/s^2$, p is the pressure of the drill-grout at a specific depth $[kPa]$, D is the depth of the drill-grout and V is the volumetric weight of the drill-grout $[kg/m^3]$. The specific weight of drill-grout is $1110kg/m^3$. The static pressure distribution over a depth of 30 meters is given in table 1.

Depth [m]	1	2	3	4	5	6	7	8	9	10	11	12	13	14	15
Pressure [kPa]	10.89	21.78	32.67	43.56	54.45	65.33	76.22	87.11	98.00	108.9	119.8	130.7	141.6	152.4	163.3
Depth [m]	16	17	18	19	20	21	22	23	24	25	26	27	28	29	30
Pressure [kPa]	174.2	185.1	196.0	206.9	217.8	228.7	239.6	250.4	261.3	272.2	283.1	294.0	304.9	315.8	326.7

Table 1: Drill-grout pressure during hardening over the depth of the borehole

The drill-grout pressure will be higher during the injection phase, but this is neglected for now since the time span of injection (4 hours) is very short compared to the time span of hardening (28 days).

2.2 Drilling fluids

For any HDD drilling, one must remain borehole stability and remove the cuttings. To achieve this, drilling fluids are used. Many fluids like oil or even water can be used, but they are, for various reasons, unfavourable. A bentonite slurry however has such properties that it meets both of these requirements and more. Together with its relative low cost and low environmental impacts it is the number 1 choice for almost every HDD project. This is why Bentonite slurry is used for this research.

2.2.1 Mineralogy

Clay is a fine grained material that exists, like all clay types, out of minerals. There are many different clay types with varying properties dependent on the type of clay minerals and their structures. One of the minerals that bentonite mainly consists of is montmorillonite (MMT). MMT is a member of the smectite group and can exist in a variety of forms. MMT is a mineral that is build up out of a sheet of alumina octahedral minerals "sandwiched" between two sheets of tetrahedral silica minerals (see Figure 4). The length of the tetrahedral and octahedral sheets can have are much longer compared to their thickness. This is why the shape of MMT crystals is described as a platelet. The structure is also referred to as a 2:1 clay. The MMT crystals in bentonite are negatively charged on the tetrahedral side of the platelets. This is caused by the exchange of Al(3+) ions with ions that have a lower charge like for example Mg(2+) and/or Fe(2+)[18].

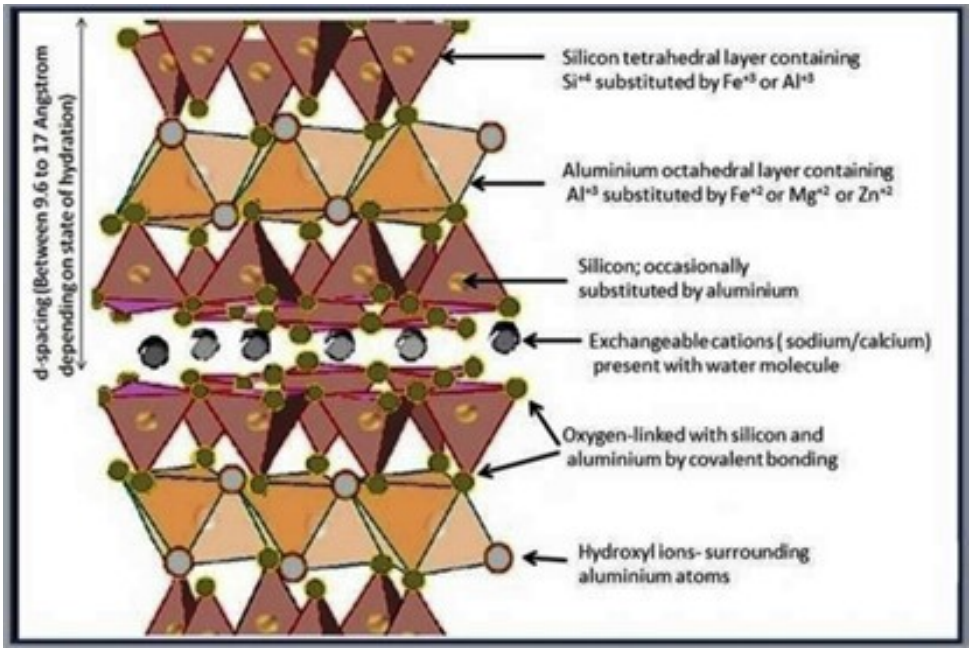

Figure 4: Schematic representation of a montmorillonite (MMT) crystal [7]

Since these bentonite MMT platelets are negatively charged at the tetrahedral end they hold, most commonly, sodium or calcium cations to obtain electroneutrality. Generally, sodium holding MMT crystals have more swelling capacity than calcium holding MMT crystals[18]. The force that keeps the platelets together is the "van der Waals force". The tetrahedral sides of the platelets is negatively charged. Thus, water, being dipolar, is attracted into the space between the platelets. Since the van der Waals force is a relatively weak force, the attraction force is able to overcome the van der Waals force and push the platelets away from each other so that the water can occupy the space in between the platelets. This phenomenon causes the clay to swell in the presence of water. This process is not sufficient to incorperate the bentonite into the water in such a way that it is suitable as a drilling fluid. To obtain the colloid structure a certain amount of mechanical energy is needed. This is why the drilling fluid is always created with mixing units.

2.2.2 Thixotropy

Bentonite slurry is a thixotropic fluid. Thixotropy is a phenomenon where the structure of a fluid is broken down under stress and rebuild at rest [3]. In other words, the viscosity of the fluid is time dependent. At rest, bentonite will behave like a solid clay. But when a certain shear stress is reached, the particle structure will break and the material will effectively lose all of its shear strength and behave like a fluid.

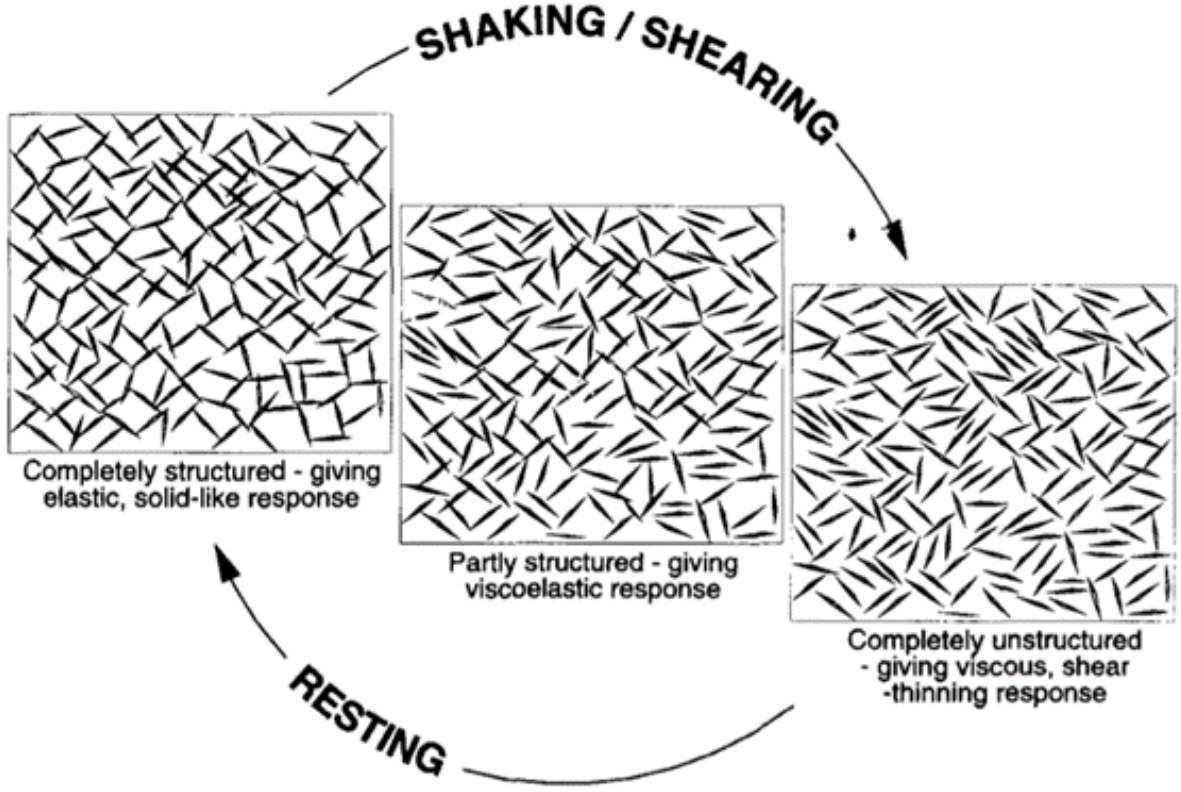

Figure 5: breakdown of a 3D thixotropic structure [3]

2.2.3 Building material

Due to the bonds between the platelets and the water molecules, the MMT platelets are able to obtain a colloid structure in the water. This structure gives the "slurry" a considerable viscosity and bearing capacity for the excavated soil particles (also known as cuttings). The presence of calcium or other salts can have a major effect on the bearing capacity of bentonite slurry because they disturb the colloid structure of the mixture. The bentonite is able to create a colloid structure because of the hydrogen bonds between the water molecules and the platelets. The charge of the ions will disturb these bonds and large salt concentration could even cause flocculation. The material for the drilling fluid is delivered in bags that contains mainly bentonite powder with some additives that are kept secret by the suppliers. The contractor will add an amount of water dependent on the desired consistency of the drilling fluid. These two components must be mixed with a sufficient amount of mechanical energy to form the drilling fluid. For this, special equipment is used. Dependent on the bentonite water ratio, a certain fluid thickness is obtained. The density will vary from 1.02 kg/L for 30 kg/m3 bentonite to 1.04 kg/L for 60 kg/m3. The higher the concentration of bentonite particles, the faster these pores will be filled with a filter cake. The filter cake will prevent fluid infiltration into the surrounding soil. Because a certain quantity of water and bentonite particles will always seep into the pores of the surrounding soil, fluid loss will always occur. Nevertheless the amount of fluid loss must be kept as low as possible. Fluid loss can be measured and it is good indicator for if there is something wrong with the borehole. For example a high quantity of fluid loss could indicate a blow out.

2.2.4 Filter cake

The fluid pressure in the borehole will be higher than the pore pressure of the soil surrounding the borehole. This over pressure will cause the fluid to flow into the pores of the soil. This process is called infiltration. Due to the over pressure in the borehole, bentonite platelets will be pushed into the pores of the soil. These bentonite platelets will constipate the pores of the soil which causes them to form a membrane on the borehole wall. The over pressure will cause the bentonite particles, together with the cuttings, to bind chemically (due to the polarity of their edges) and mechanically (because of the over pressure in the borehole) along the borehole wall to form a filter cake [23] (see figure 6a). A filter cake is critical for the borehole stability. It forms a layer

with a very low permeability which enables a high borehole pressure with a limited increase in pore pressure in the surrounding soil. In a situation without a filter cake, the pore pressure in the soil could rise to a point where liquefaction would occur which would most likely result in the collapse of the borehole. Thereby there would be a substantial quantity of fluid loss because of infiltration in the surrounding soil. Since this filter cake will form as a uniform layer over the borehole wall, it will have its own parameters just as any other soil. Wang & Sterling [2007] took the following parameters into account for their research: a friction angle of 25 degrees, a cohesion of 138 kPa and a density of 1474 kg/m3 [23]. Although some research has been done, it is not well known what the parameters are for any type of filter cake that is formed by bentonite slurry in any soil. Also, the typical depth of bentonite slurry intrusion in the soil could have a major impact on the behaviour of the filter cake and the soil in the borehole wall.

A filter cake consists of two layers. The first layer is formed as the drilling fluid enters the borehole and thus is the "inner layer". The second layer is formed as the drilling fluid is leaving the borehole and thus is called the "outer layer". Since the filter cake thickness and composition is dependend on many factors (mixing water composition, soil porosity, drilling fluid concenrations etc.) it is hard to say what a filter cake will look like. To give a general indication, in an average sand, the thickness of the filter cake could reach around 1.5 mm [20]. Three different types of filter cake can be distinguished and the type of filter cake formed is dependent on the slurry particle size and slurry density. The types of filter cakes are a filter cake with hardly any infiltration (type a), a filter cake with an infiltrated zone (type b) and only an infiltration zone without a filter cake (type c) (see figure 6b) [12]. Yin et. al [2021] have made a model to visualize the infiltration and under which circumstances a certain type of filter cake develops. They discovered how the particle diameter and cohesion energy determine the type and depth of filtration [27].

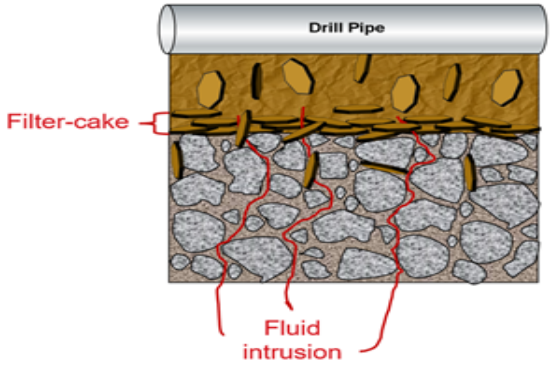

(a) Representation of filter cake and intrusion. Figure is created and owned by CEBO.

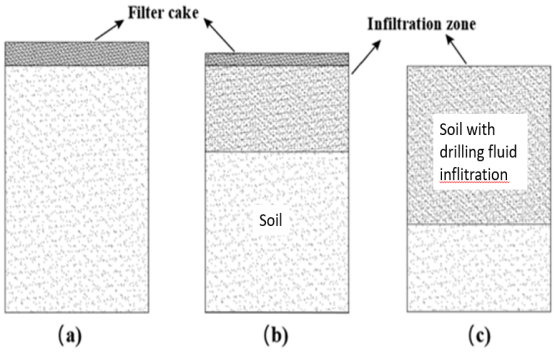

(b) 3 different types of filter cakes [20]

Figure 6: Filter cake

2.3 Drill-grout

Drill-grout is used for permanently sealing a borehole. Drill-grout can be any grout type used in drilling projects, but often a grout bentonite mixture is used. The key raw materials used to make grout is cement, which is made from limestone and clay. Together they are burned at around 1400 degrees Celsius to form clinker. These clinkers are then pulverised to powder which we call cement. One of the mainly used cements is Portland cement, named after the Portland cliffs[19] which was, at the time, regarded to as the strongest building material. When cement is mixed with water hydration will take place. Hydration is a chemical reaction which, in the case of cement, will cause the formation of crystals. These crystals will connect and grow into each other. This will cause the cement to harden and form its strength.

When a borehole is sealed to prevent seepage, a water impermeable material is needed. To prevent any flow of water along the length of the borehole, the borehole must be filled with a material that has a strength sufficient to resits the hydraulic head of the surrounding aquifers. Also, this material must be able to prevent settlement. Grout is a material that could meet these requirements but it is unable to hydrate sufficiently. This is because the static pressure of the cement water emulsion is larger than the surrounding hydrostatic pressure (assuming normal conditions). When the cement column is deep enough, this pressure difference will cause the water to be pressed out of the grout column leaving too little water for the grout to hydrate sufficiently. A weak and brittle

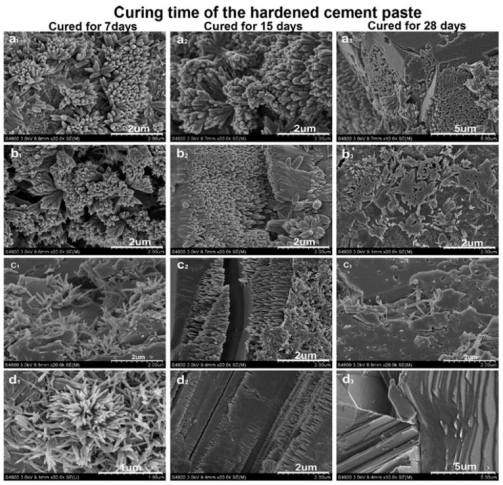

Figure 7: SEM images representing cement hydration crystals at differ GO concentration [9].

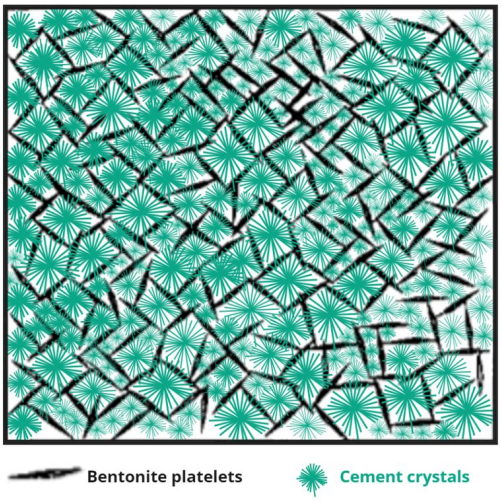

Figure 8: schematic representation of how the bentonite forms a skeleton in the drill-grout mixture. Edited picture from Barnes 1997 [3]

grout will be formed that is unable to seal the borehole water tight. Another downside to grout is that it is very hard to cast it into the small area between the borehole wall and the constructed pipe. All of these problems can be solved by mixing the cement with bentonite. Drill-grout is a grout where bentonite has been added up to a maximum of 75% grout and 25% bentonite [5]. There is no specific rule for the bentonite grout concentration and lots of varieties can be used or designed for specific projects. If the contractor has drilled correctly, the drilling fluid should have formed a filter cake that is able to hold most of the drill grout in place. The advantage of the bentonite is that the bentonite will form a skeleton that keeps the grout and water particles in their place which enables the grout to hydrate sufficiently (see Figure 5). The downside of this structure is that there is a large reduction in shear strength of the drill-grout (22,0 kPa) [5] in comparison to regular grout (in the order of 3 to 4 MPa[1]).

According to CEBO (the distributor of the drill-grout that is used in over 90 percent of the market), the drill grout is regarded to as fully hydrated after 28 days. In reality the hydration reaction should be twice as long but the shear strength will not increase sufficiently by this. The drill grout will have become a plastic formation with a permeability comparable to most clay types (1*10-9 m/s). Because the material is plastic it will lose its strength after deformation. If, for example, a crack has been formed due to deformations, the drill-grout is able to heal itself by filling the crack with its own material. Due to the surrounding water and the swelling properties of bentonite, the drill-grout will swell back into the formed cracks sealing it water tight. The Bentonite will also push some cement crystals into the cracks which will give the material a certain strength which is higher than bentonite, but lower than the original material. This is because the cement crystals do not form a continuous body throughout the crack, but it will rather contain loose cement crystals mixed in a bentonite paste (see Figure 6). For further knowledge about the strength of drill-grout under repeated deformations it is important to find the strength after certain plastic deformations.

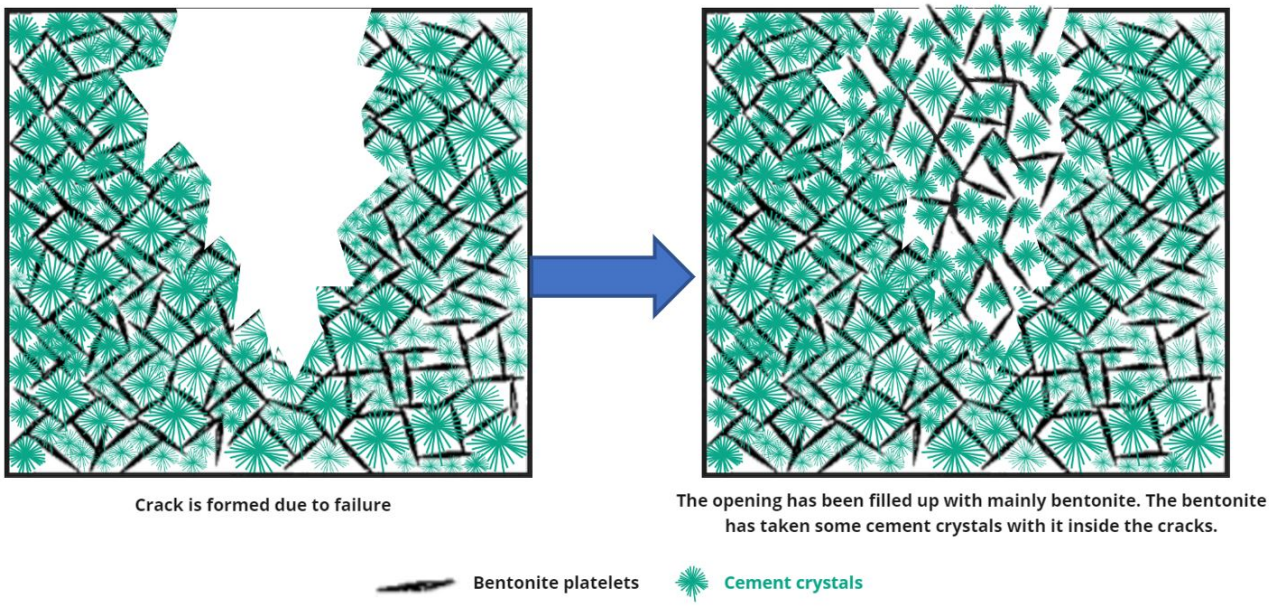

Figure 9: schematic representation of how drill-grout can be partly "self healing". Adapted figure from Barnes 1997 [3]

2.4 Medium pipe

Concerning the construction of heat transportation pipes, the contractor generally has 3 options.

The first option is the flex pipe. The flex pipe is shaped like the hose of a vacuum cleaner. Due to its shape it has extra flexibility which makes them suitable for projects with high borehole angles. The maximum thickness at which the flex pipe is manufactured is 200 mm.

The second option is the steel in steel pipe. The steel in steel pipe is able to cover further distances in a single drill relative to any other pipe used for heat transportation. The steel in steel pipe has a lower expansion due to temperature changes but it is a relatively expensive option.

The third and last option is the steel-pur-PE pipe. This option is explained in the introduction.

2.5 Friction

2.5.1 Roughness

The roughness of the borehole has to be investigated since this affects the interface friction greatly. It is important to know exactly what kind of roughness the borehole could have and how it can affect the interface friction. In the following subsections the roughness is subdivided into micro- and macro-scale. The micro scale is the surface roughness caused by the particle size and variation. For this a length of 10 mm borehole surface in the longitudinal direction is chosen to be considered. This length is arbitrary and chosen because it is about 10 times the length of a sand particle and thus only the roughness caused by the particle sizes is considered. The macro-scale roughness is caused by the reaming process and soil collapse inside the borehole and considers irregularities of the borehole radius over the entire length of the borehole.

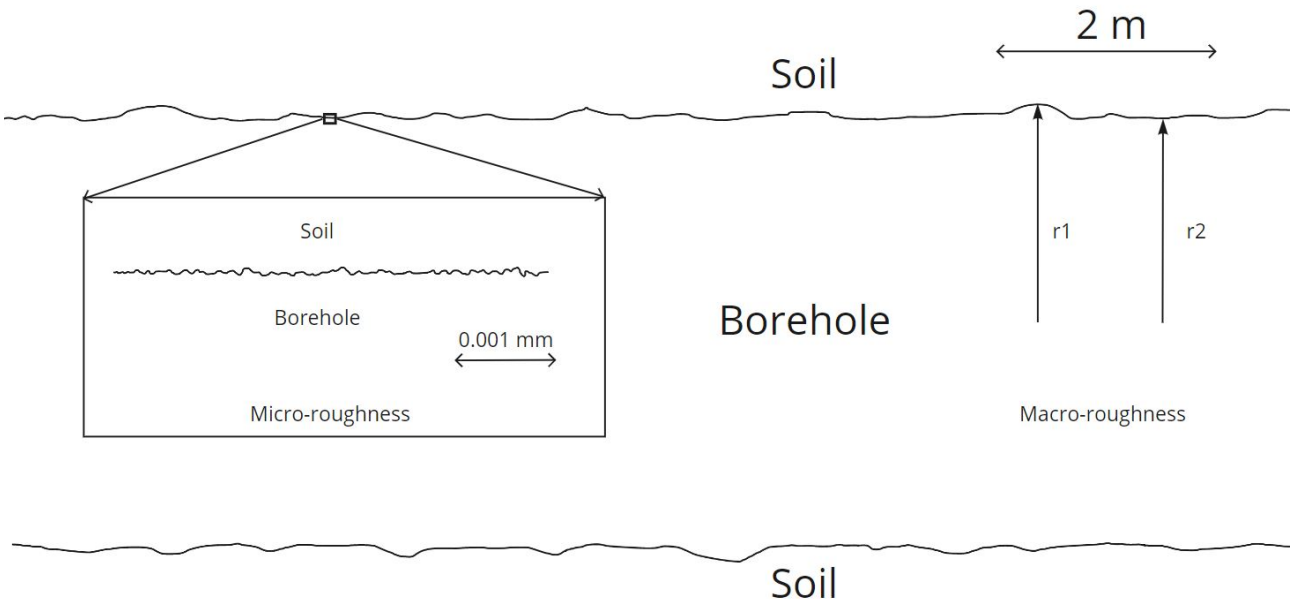

Figure 10: Visualisation of macro- and micro-roughness

2.5.2 Micro-scale roughness

When investigating the micro-scale roughness, only the average roughness parameter R_a will be considered. This roughness parameter is calculated by hand of the following formula: $R_{n,a} = R_a/D_{50}$ where, R_a is the average centreline roughness, $R_{n,a}$ is the normalised roughness parameter and D_{50} is the mean particle diameter. According to Martinez's and Frosts research (fig. 11)[10], the roughness of the sample has a significant effect on the interface friction angle but up to a maximum of where the interface friction angle is equal to the internal friction angle of the specimen ($\delta = \phi$). This point is reached when the roughness parameter is greater than 2 mm.

2.5.3 Macro-scale roughness

Generally, the reaming process will make sure that the change of the radius over the length of the borehole is small. Nevertheless, since soil collapse can still occur and cause variations in the borehole radius. The change of radius along the borehole and its effect on the interface friction has to be investigated.

No literature has be found yet about how the interface friction of soil is dependent on the macro-scale roughness. A research is proposed to create a macro scale roughness and do a test to see how the interface friction will change. Untill now it is presumed that the macro scale roughness is be comparable to the structured roughness that was researched by Martinez and Frost[10].

2.6 Bentonite and drill-grout intrusion

Even when a filter cake is formed, there is always infiltration of the drilling fluids into the soil. This will affect certain parameters like the cohesion, permeability and internal friction angle. The length of intrusion is dependent on multiple factors like porosity, permeability, borehole pressure, drilling fluid density and many more. Because the infiltration depth is dependent on so many factors it is very hard to model a realistic soil behaviour when there has been bentonite infiltration. Many parameters are unknown and there are always unexpected scenario's that can have an influence on the drilling fluid rheology and the subsurface.

2.6.1 Borehole pressure

The bentonite pressure in the borehole must be sufficient to prevent soil collapse and it must not be too high to prevent a blow out. A soil collapse causes an increase in macro roughness and a blow out breaks up the

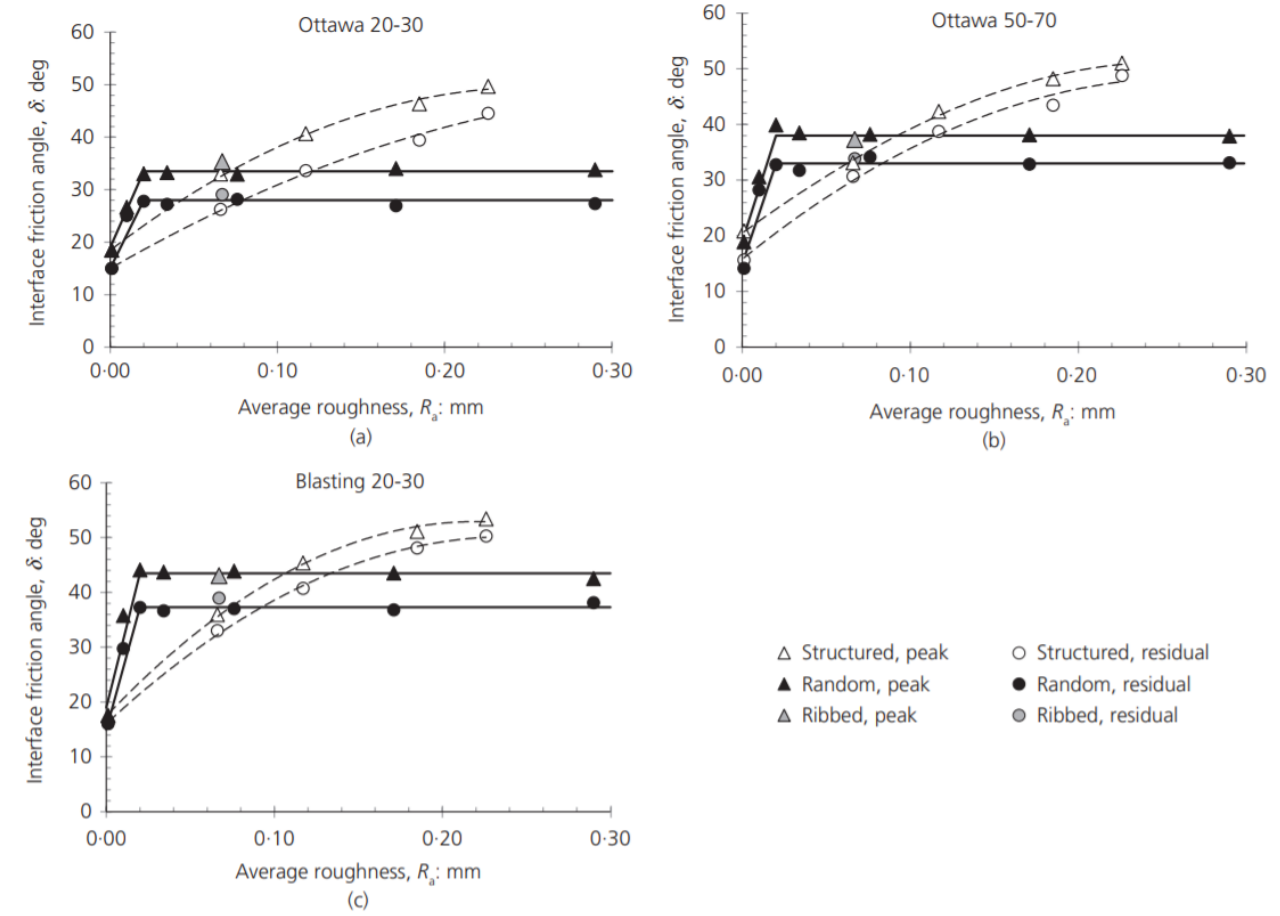

Fig. 4. Measured IF angles for tests on (a) Ottawa 20-30, (c) Ottawa 50-70 and (d) Blasting 20-30 sands

Figure 11: From Martinez's and Frosts research about the influence of surface roughness form on the strength of sand-structure interfaces[10]

soil structure which causes a decrease in soil strength which also causes soil collapse. A study to formation fracturing in an HDD project in China shows that the pressure in the borehole was between approximately 700 kPa and 2100 kPa[25]. They have done an analysis with a finite element model to investigate how large the plastic zone is around the borehole. This plastic zone was in some places so large that it reached the surface. Still, one picture shows that the borehole still had a round shape which means that there was not a large amount of soil collapse near the exit of the borehole.

2.6.2 Soil infiltration

If the soil is porous enough, the drill fluid and drill-grout could infiltrate the soil to form an internal cake. This internal cake will create a layer that contains a mixture of soil and drill fluid / drill grout. This could could have a significant effect on the sliding mechanism between the drill-grout and soil. CEBO claims that the infiltration is insignificant even under higher pressures. This claim is founded on experience and data gained from the field.

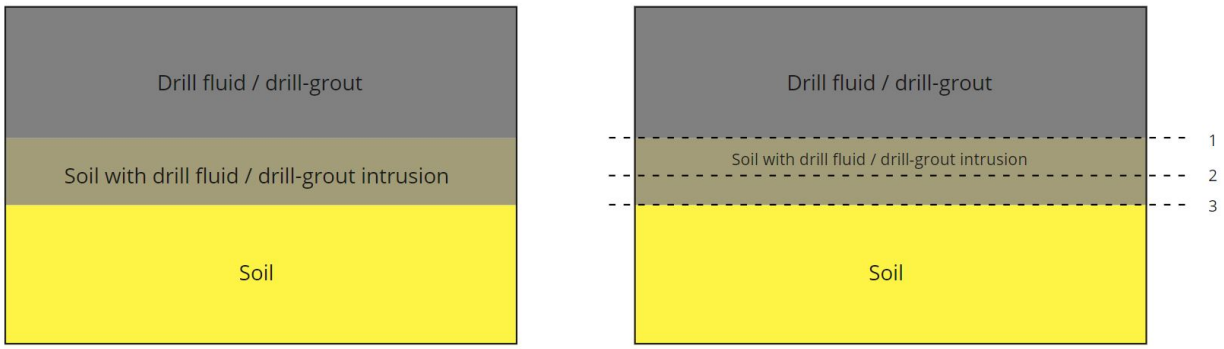

Figure 12: Schematic representation of soil intrusion by drill-grout of drilling fluid. The dotted line shows potential sliding planes for the DST test.

Sacremento et. al (2014), have done research about the deep bed filtration of two size particle suspensions in porous media. They state that the thickness of the dril fluid intrusion $z(T)$ is calculated from

$$z(T) = \frac{D_1 + 1}{\lambda_c} ln[(1 - \frac{c_3^0 exp(-((\lambda_c D_1)/(D_1 + 1))T_{tr})}{(1 - \phi_2)D_1} exp(\frac{\lambda_c D_1}{D_1 + 1}T) + \frac{c_3^0}{(1 - \phi_2)D_1}] - D_1 T \tag{2}$$

Where, $z(T)$ is the internal cake front location, T is the time and T_{tr} is the transition time. D_1 corresponds to the speed of external filter cake built of the large particles. It is obtained from the mass conservation of injected large particles: $\phi_3 c_0^2/(1 - \phi_3)$ where ϕ_3 is the external cake porosity and c_0^2 is the initial particle concentration. λ is the dimensionless filtration coefficient, which is denoted as λ_c for the filter cake. c_0^3 is the injected small particle concentration. ϕ_2 is the porosity of the internal cake formed by the small particles [17].

Müller-Kirchenbauer (1977) and Kilchert Karstedt (1984) have also done research about this and they've obtained a formula that is much easier to use and more fitting for this research. They claim that the maximal penetration distance is dependent on the total pressure difference over the filter cake Δp_s, the seive size of which 10% of the mass of the particles passes d_{10}, shear strength of the bentonite τ_F and the relation between the grain size and the effective radius of a flow channel α[8][13][4].

$$e_{max} = \frac{\Delta p_s d_{10}}{\alpha \tau_F} \tag{3}$$

Since most of these parameters cannot be accurately determined it not possible to make an estimated guess of the drill fluid / drill grout intrusion with Sacremento's method. However, the method developed by Müller-Kirchenbauer (1977) and Kilchert Karstedt (1984) can be used to make an estimated guess of the amount of bentonite intrusion into the soil body should it be found interesting for the research.

Research plan

For this research, 2 tests were performed. A direct shear test and a self designed test which is named the dynamic pipe interaction test (DPIT). The DPIT method included a self made sample making device and a pulling machine that measured force in Newtons and distance in millimetres. Out of these results a conclusion was drawn. In this chapter, first the two methods are described. After this, it is described how the samples are created. Lastly, the methodology of the test performance is explained.

3 Test methods

3.1 Shear test

The direct shear test (DST) was done with the help of a shear box. An example of the shear box that was used is shown in figure 13. The DST is a test method that can be used to find shear strength properties of a material. The test is performed with the help of a shear box. The shear box is a tool that allows the material to be sheared while measuring the load that is applied while shearing.

A DS test will be used to find the interface friction angle between drill-grout and sand. A drill-grout sample will have to be made that fits precisely inside the lower half of the shear box. It is very important that the shear zone surface lies exactly between the drill-grout and the sand sample. Another point to note is that the friction angle is largely dependent on the roughness of the drill-grout sample. The potential effect of the roughness on the friction angle is researched in chapter ("friction").

To ensure that the roughness of the drill-grout sample matches the roughness of the soil, the drill-grout will be cast on to the sand. The shear box of the DS test will be used as a mold. Because drill-grout takes over 28 days to harden to its full strength, it is placed in the oven under 40 degrees Celsius. According to CEBO (the supplier of the drill-grout used in the experiments) the drill-grout will take 40 hours in a 40 °C environment to harden to the same strength as it would in a normal environment after 28 days.

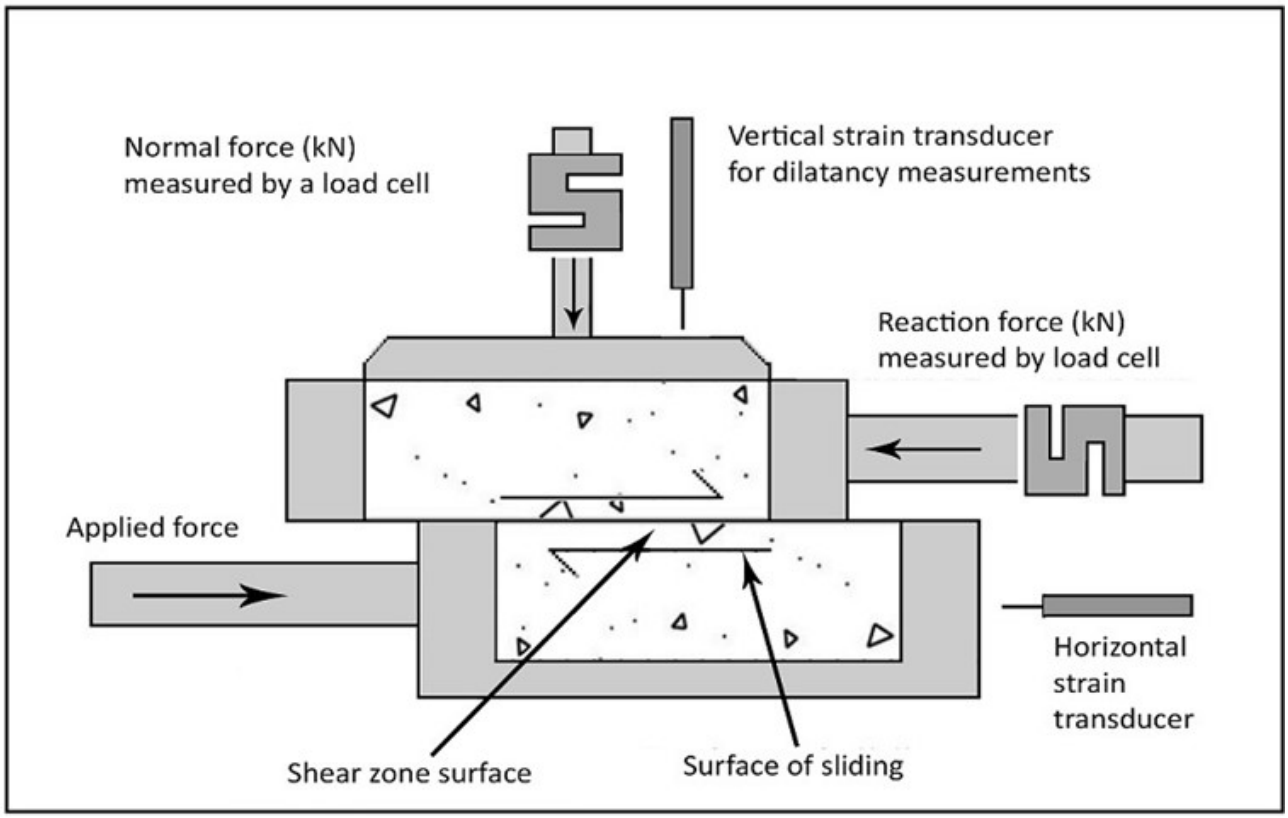

Figure 13: schematic representation of a possible shear box. In this case, drill-grout could be either at the top part or the bottom part of the shear box.

3.2 Dynamic pipe interaction method

Unfortunately, the DS-test is not able to mimic a realistic situation. In a realistic situation, a filter cake is formed due to the use of a drilling fluid. This filter cake can be located in the soil body and on the soil body in the bore hole. After this, the drilling fluid is replaced by the drill-grout. Due to these processes, a complex and multi parameter dependent soil formation is created (see Figure 14).

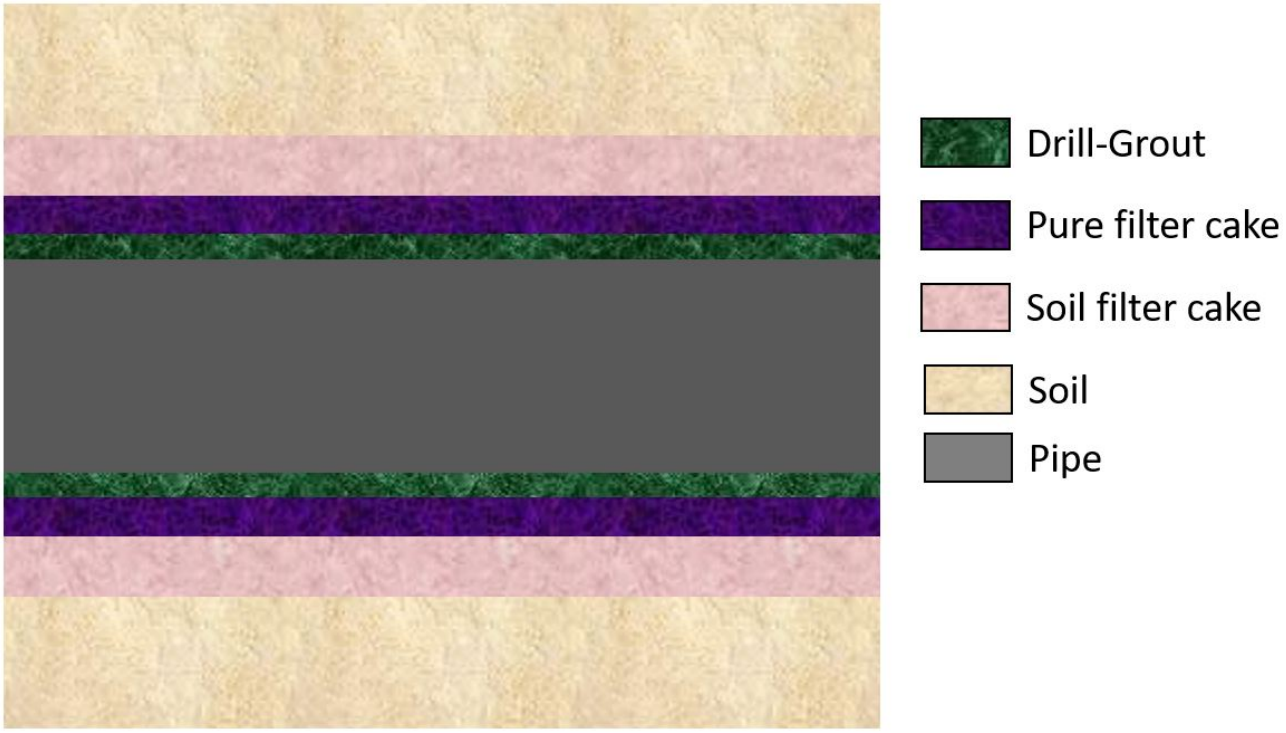

Figure 14: crossection of a borehole filled with drill-grout.

The strength and friction characters of the drill-grout can vary based on its design. Every supplier makes its own drill-grout and specific drill-grout mixtures can be created for a certain project. The pure filter cake and soil filter cake is dependent on the drilling fluid, borehole pressure and certain soil parameters. The soil parameters that can affect the filter cake are salinity, grain size, grain size distribution, porosity and permeability. Further research about the specific effect of each of these parameters to the creation of the filter cake still has to be done. The pure filter cake and soil filter cake can be altered by each of these parameters independently, meaning that one parameter may or may not have an effect on either the soil filter cake or the pure filter cake dependent on the other parameters. And finally, the internal and interface friction angle could be dependent on the filter cake. Summarised, the geology in and around the borehole is altered to such a level that there is no theory available yet to estimate its effect to the interface friction angle between the drill-grout and soil. This is why the soil formation has to be recreated as accurately as possible so that the effects can be measured. To do this, a new research method has been developed. A setup is made that will be called the "Dynamic Pipe Interaction Application" (DPIA).

3.2.1 How the DPIA is built

The DPIA has been specifically designed to recreate a borehole that is dug with trenchless technologies. At the end of the sample making process there will be two distinct types of materials: the static material and the dynamic material. The static material will stay fixed in placed while the dynamic material is being pulled out of the static material, hence their names static and dynamic. To explain how the DPIA works, its is best to firstly consider it part by part.

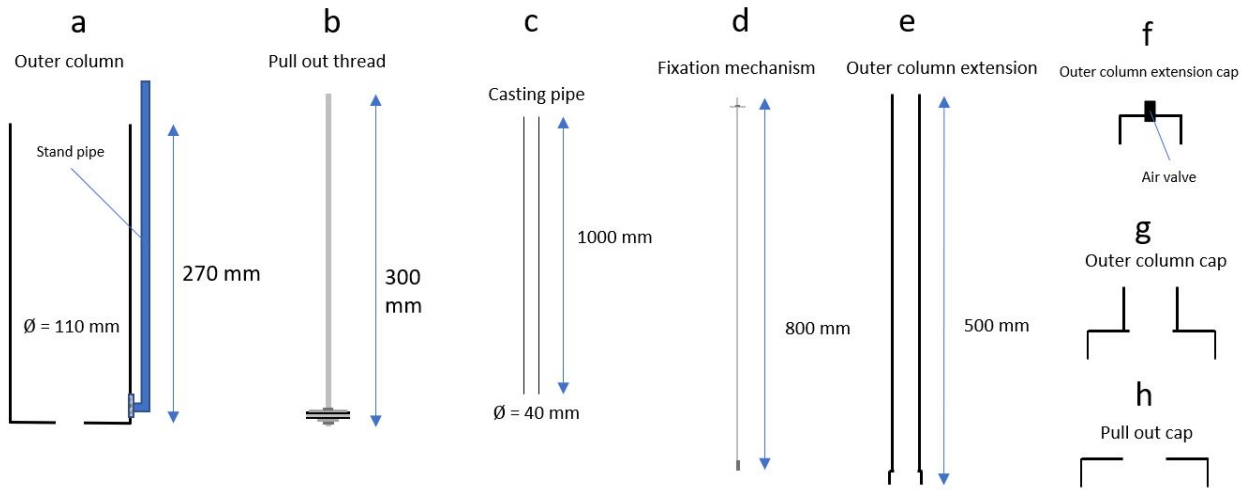

Figure 15: 2D representations of the parts of the DPIA. Please note that these drawings are cross sections and that in 3D they are all cylindrical.

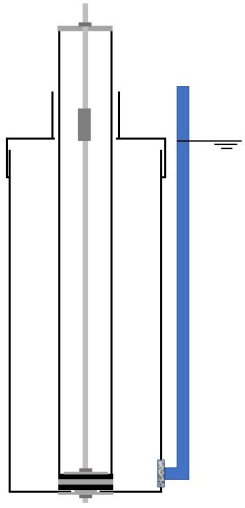

Figure 16: 2D representations of the fully assembled DPIA.

The outer column (Figure 15 a) is a hollow pipe where in the static material is placed. There is a air hole in the bottom to prevent a vacuum while pulling out the dynamic material. There is also a stand pipe that allows water to flow out of the outer column while the system is pressurised. A filter is placed at the beginning of the standpipe to prevent any particles larger than the size of silt from flowing out of the outer column.
The pull out thread (Figure 15b) is used for pulling out the dynamic material. It is made up of three circular iron discs and two rubber circular discs that are stacked on top of each other. Each of these discs are described from bottom to top:

At the bottom is an iron disc that provides support to the rubber discs that is situated above. The bottom disc has a diameter of 30 mm and is just smaller than the air hole at the bottom of the outer column. The rubber disc placed on top of the smaller iron disc has a diameter of 40 mm and seals the outer column so that neither water nor air is able to flow out. On top of the bottom rubber disc there is a iron support disc with a diameter of 40 mm. This disc supports the 40 mm diameter rubber disc that lies on top of it. The top rubber disc is used to seal the casting pipe so that no water or static material is able to flow into the casting pipe. The top disc is made from iron again and it has a diameter equal to the inner diameter of the casting pipe which is about 37 mm. This disc is used to provide both support to the rubber discs as to keep the casting pipe in

place. The discs are held together with two bolts.
The casting pipe (Figure 15c) is a meter long pipe used for casting the dynamic material. It is pressed firmly on the rubber disc of the pull out thread with the fixation mechanism. The fixation mechanism (Figure 15d) can be screwed on top of the pull out thread. At the top of the fixation mechanism is an iron disc with the same diameter as the casting pipe. This disc can be screwed tightly on op of the casting pipe so that the flow from the outer column to the casting pipe is made impossible.
The outer column cap (Figure 15g) can be screwed on top of the outer column. The chimney on top of the cap has a inner diameter of 40 mm at the bottom and 45 mm at the top. Because of this it can be shoved over the casting pipe while keeping the friction low enough so that the casting pipe can be pulled out by hand. This is very important since particles will get stuck in between the casting pipe and the inner wall of the chimney.
The outer column extension (Figure 15e) can be screwed on top of the chimney and its purpose is to retain the material that is poured into the casting pipe. Otherwise, when the casting pipe is removed, the material would spill. This pipe has a special cap with an air valve (Figure 15f) so that the system can be pressurised.
At last there is a cap with a hole of 40 mm diameter (Figure 15h) that can be screwed on top of the outer column. In the pull out phase of the experiment, this cap is used to keep the static material in the outer column while the dynamic material can pass trough the hole that is in the centre of the cap.

3.3 Sample preparation

3.3.1 Direct shear test

The initial plan was to make the samples shown in table 2. This would be done as follows:

Sample type	Sample amount
Sand	3
Clay	3
Drill-grout	3
Sand - drill-grout	6
Sand - drill-grout with vertical pressure	3
Clay - drill-grout	6
Clay - drill-grout with vertical pressure	3
Drill-grout - PE	6
PE - PUR	6
PUR - metal	6

Table 2: Type and quantity of the samples that are made

Sand: The sand used for this experiment is Merwede sand (river sand). The sand is put into the container and then it is pressed by hand. 2 different kind of samples will be made: a rough sample and a smooth sample. The smooth sample will be compressed with a smooth surface and the rough sample will be compressed with a rough surface. The casting and compression mechanism is made clear in figure 17.

Clay: The clay type used for this experiment will be a medium strong clay. Only smooth clay samples will be used in this experiment. The clay samples will be made by filling the container with clay and striking the excess clay off.

Drill-grout: The drill-grout samples will be cast to the shape that is needed for the DS test and dried at 40 °C for a minimum of 44 hours so that the sample has the same yield stress as after 28 days of hardening.

Sand - drill-grout: A layer of sand is made on the bottom of the container. On this sand layer the drill-grout will be cast. This container will now be sealed air tight and put into the oven on 40 °C for a minimum of 44 hours to harden. The same sample will be made with a vertical load of approximately 1 kg applied on top of the drill-grout.

Clay - drill-grout: A layer of clay is made on the bottom of the container. On this sand layer the drill-grout will be cast. This container will now be sealed air tight and put into the oven on 40 °C for a minimum of 44 hours to harden. The same sample will be made with a vertical load of 1 kg applied on top of the drill-grout.

Drill-grout - PE: A flat piece of PE will be put in the container on which drill grout will be cast. This container will now be sealed air tight and put into the oven on 40 °C for a minimum of 44 hours to harden.

PE - PUR: A flat piece of PE will be put in the container on which PUR will be cast.

PUR - metal: A flat piece of metal will be put in the container on which PUR will be cast.

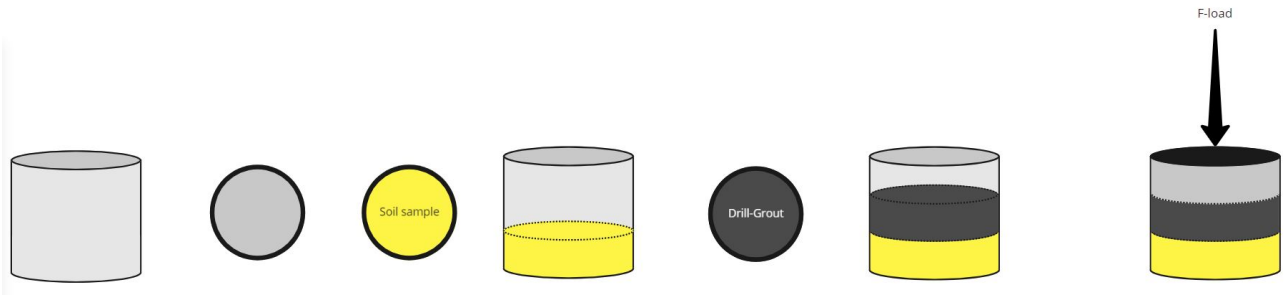

Figure 17: Overview of the sample making progress considering soil and drill grout.

3.3.2 DPIM

First the pull out thread is placed in the centre of the outer column. It must be screwed tight with the help of a 40 mm iron disc. The casting pipe is placed on top of the pull out thread and screwed tight with the help of the fixation mechanism. All parts should be fixed firmly. The outer column can now be filled with the desired material. Make sure that the outer column is filled up on to 1 cm below the top of the column so that there is enough space for the cap to be screwed on. Put the outer column cap over the casting pipe and pull it downwards and screw it tightly. Screw the outer column extension on the outer column cap. Make sure that the drilling fluid is ready to be poured into the casting pipe. Remove the fixation mechanism and fill the casting pipe with the drilling fluid. Remove the casting pipe and place the outer column extension cap on the outer column extension. Apply up to 0.5 bar of air pressure on the air valve in the outer column extension cap and wait until the flow of fluid out of the stand pipe is negligible. Remove the outer column extension and prepare the drill grout. When the drill grout is ready it can be poured into the inner column. Since drill grout has a greater density than bentonite fluid it can replace the drilling fluid when it is squirted via a tube at the bottom of the column. After all of the drilling fluid is replaced with drill grout, the cap can be screwed on the outer column cap so that the whole system is sealed air tight. The samples can be put into the oven on 40 degrees Celsius for 40 hours, or left to dry in room temperature for 30 days.

3.4 Methodology

3.4.1 Shear test

The shear test is executed in the lab with the help of a shear box. The soil is placed at the bottom and the drill-grout is placed on top. This way the shear zone surface will be constantly in between the two moving parts of the shear box. A force normal to the sliding plane is applied before the start of the test. After the measured shear force is no longer increasing and thus stays constant, the normal force will be increased. This last step can be repeated as many times as seems needed. In this case the normal force was increased two times. See figure 13 for a sketch of the set-up.

With this method, 3 parameters are measured. A vertical displacement, a horizontal displacement and a shear force. The normal force is arbitrary. The results of these tests can then be used to calculate the soil parameters.

3.4.2 DPIM

The pull out phase is the phase after the samples have either hydrated for at least 48 hours in a 40 degrees Celcius oven, or 28 days at room temperature. The outer column cap can be replaced with the pull out cap

and the excess drill grout is then removed. The thread of the pull out thread will be sticking out of the DPIA so that it can be attached to the pulling machine. The pulling out must be done with a constant velocity while the pulling force is measured. When the force is steadily declining, the friction is balanced and the test can be stopped. It can also be decided to continue the test until the inner column has been pulled out fully.
The friction of the system will also have to be calculated. This is done by preparing the sample without the drill grout. This is done by ending the sample making process after the drilling fluid has been pressurised. A pulling force and a displacement are measured. These will then be used to calculate the shear force between drill grout and soil and the shear force created by the system. With these results it can be calculated what shear stress is developed between drill grout and soil. Because only 4 DPIA's can be made, 4 samples can be made at the same time. These grout in these samples will be hydrated into a 40 degrees oven for at least 48 hours. To keep the time needed for the research within restraints it is chosen to only do 4 sets of tests creating data from 16 samples in total. As is said before, one of these sample sets will be made without drill grout to measure the friction of the system. After this the potential effect of the resulting shear stress can be analysed using a standard calculation for calculating the amount of expansion loops needed.

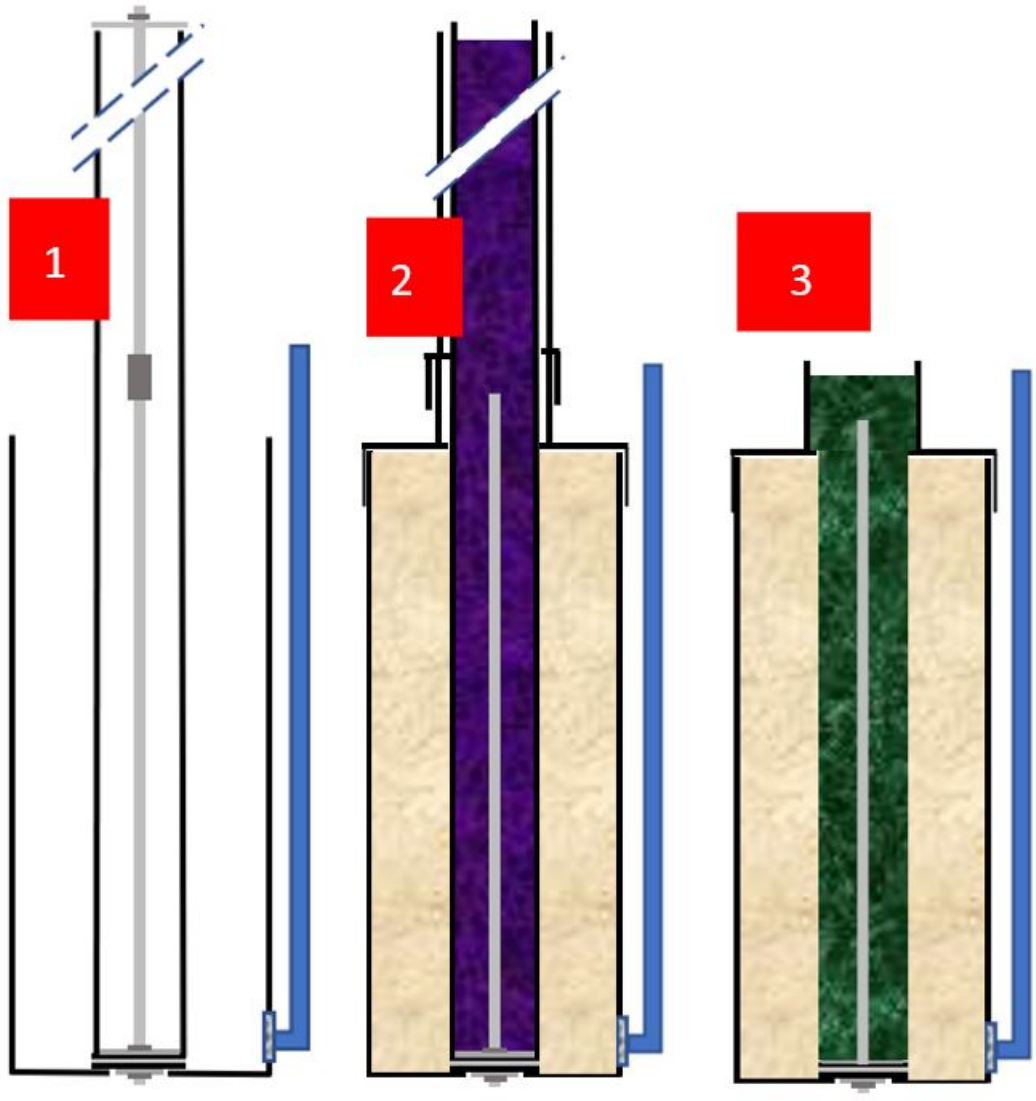

Figure 18: Representation of the sample making process.

4 Results

4.1 Direct shear test

The results of the shear test are shown in the appendix. It was chosen not to analyse them in the main report since it is concluded that they are unrealistic. This is because it was very difficult to prepare the sample such that the shear zone surface is exactly in between the drill-grout and soil. The reason for this is because the drill-grout needs to be poured onto the soil sample that will be used for the test. Soil particles will be sucked into the drill-grout at random locations which causes a non-conform surface. A second problem is that the shear zone surface will deviate from the sand-drill grout boundary. Because of this the path of the shear zone surface will be entirely through the sand and not in between the drill-grout and sand (see Figure 22). At last, the DS-test does not represent a realistic situation. In reality, there is a filter cake formed by the drilling-fluid in between the sand and drill-grout. It was not possible to create a soil – filter cake – drill-grout sample that can be used in the shear box. Because of all these difficulties a different research approach was suggested.

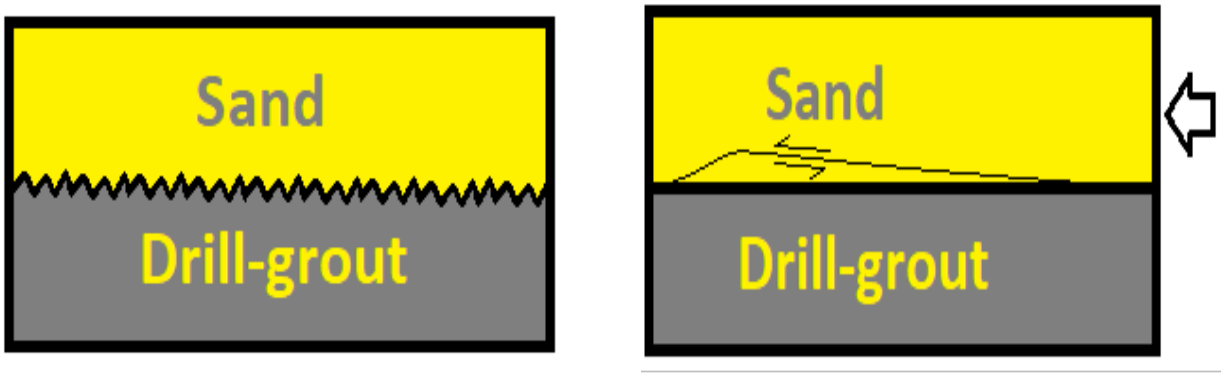

(a) Representation of the roughness of the Sand-drill-grout border.

(b) Representation of the shear zone surface during the DS-test wil sand and drill-grout.

Figure 19: DS-test difficulties

4.2 Dynamic pipe interaction method

The test results are composed of 3 parameters: a pull out force [N] that can be considered as friction, time [t] and a displacement [mm]. 4 tests consisting out of 4 samples were done. Thus, 16 results were obtained. 4 different results are shown in figure 20. The remaining results are shown in figure 38, 39, 40 and 41 in the appendix. In the figures, on the x-axis is the displacement in millimetres and on the y-axis is the force in Newton. At first sight, the plots do not seem similar at all, but a general trend can be found in most of the tests. Still, a general trend can be found in most of the tests. In most of the cases, the force needed to obtain displacement will increase until it reaches a maximum. After the maximum the force is reached, the force needed for further displacement will decrease linear until the end of the test. It is thought that in the tests where the maximum frictional force is reached after 150 mm of displacement, the force is mainly determined by the accumulation of soil particles in between the bottom pull out cylinder and the drill-grout.

4.2.1 Observations

The final samples had a thick filter cake in between the soil body and the drill grout column. This filter cake was developed by the pressurisation of the drilling fluid. The filter cake had a thickness of at least 1 millimetre. This prevented any attachment of the cement crystals with the soil particles. Figure 22a shows the cross sectional area of the sample as it was used for the pull out phase of the test. Figure 22b shows a sample where only drilling fluid was pressurised after which no drill grout has been casted. Because of this it is possible to see how thick the filter cake can become. Figure 21 shows a schematic representation of the sample shown in Figure 22a. The filter cake made any micro-scale roughness irrelevant. The cake was smooth throughout the length of sample and because of its low shear strength, any differences in the borehole diameter smaller than 1 millimetres couldn't have any effect on the roughness of the borehole wall.

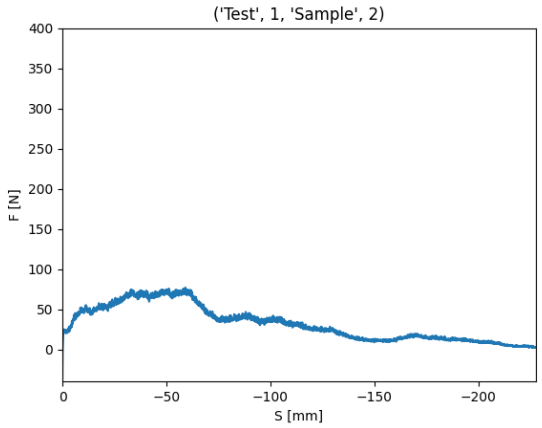

(a) Plotted results from test 1 sample 2

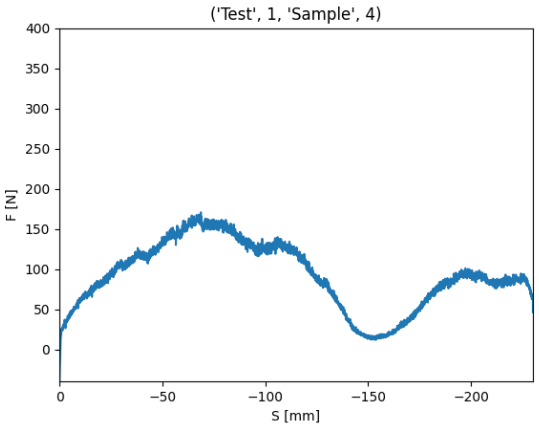

(b) Plotted results from test 1 sample 4

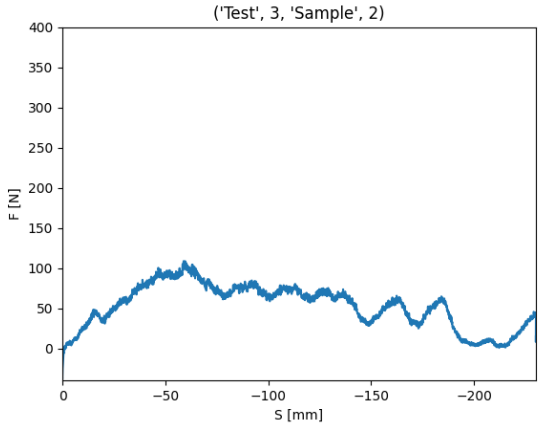

(c) Plotted results from test 3 sample 2

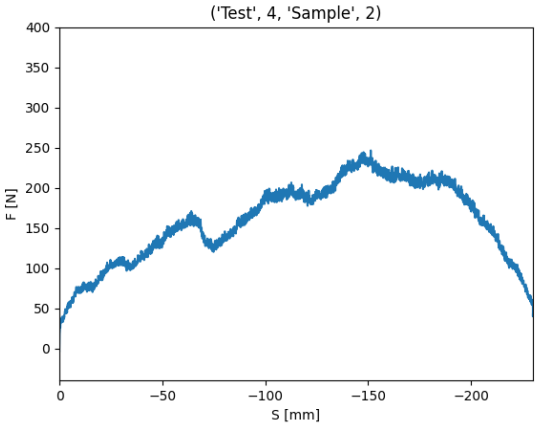

(d) Plotted results from test 4 sample 2

Figure 20: 4 plotted results from the total of 16 results

As can be seen in Figure 23b, the drill grout did not fully cover the entire length of the pull out thread. This is because some parts of the pull out thread mechanism prevents the flow of drill grout to some parts on the bottom of the pull out thread (see Figure 23a). When the pull out thread is being pulled out during the pull out phase, sand can be shaved of the borehole wall by the bottom cylinder. This sand can accumulate and replace the drilling fluid in between the drill grout and the bottom cylinder. This could cause the friction to rise significantly. Also, there could be an increase in friction when the bottom cylinder comes closer to the top of the container because the sand particles have no more space to move upwards. This could increase the amount of shearing and even faulting of the sand particles. The drill-grout in the samples of test 2 were not hardened sufficiently. Because of this, the drill-grout in the samples was very weak compared to the drill-grout in the samples from test 1 and 4. The strength of the drill-grout used in test 2 was not measured, but it was so weak that the outer part of the cylinder (about 5 millimetres thick) could be scraped off the inner part by hand. In other words, the strength could be compared with the strength of a soft clay. Figure 29b and 29a show that test 2 is still within the bounds of test 1 and test 4. The measured force was not significantly lower or higher. This implies that the strength of the drill-grout does not necessarily contribute to the friction that it has with the soil.

4.2.2 Explanation graphs

Generally, the graph of a test with the DPIA can be described as follows: The slope gradient starts positive and will deteriorate until it reaches a peak. After the peak the slope gradient becomes negative. The pull out

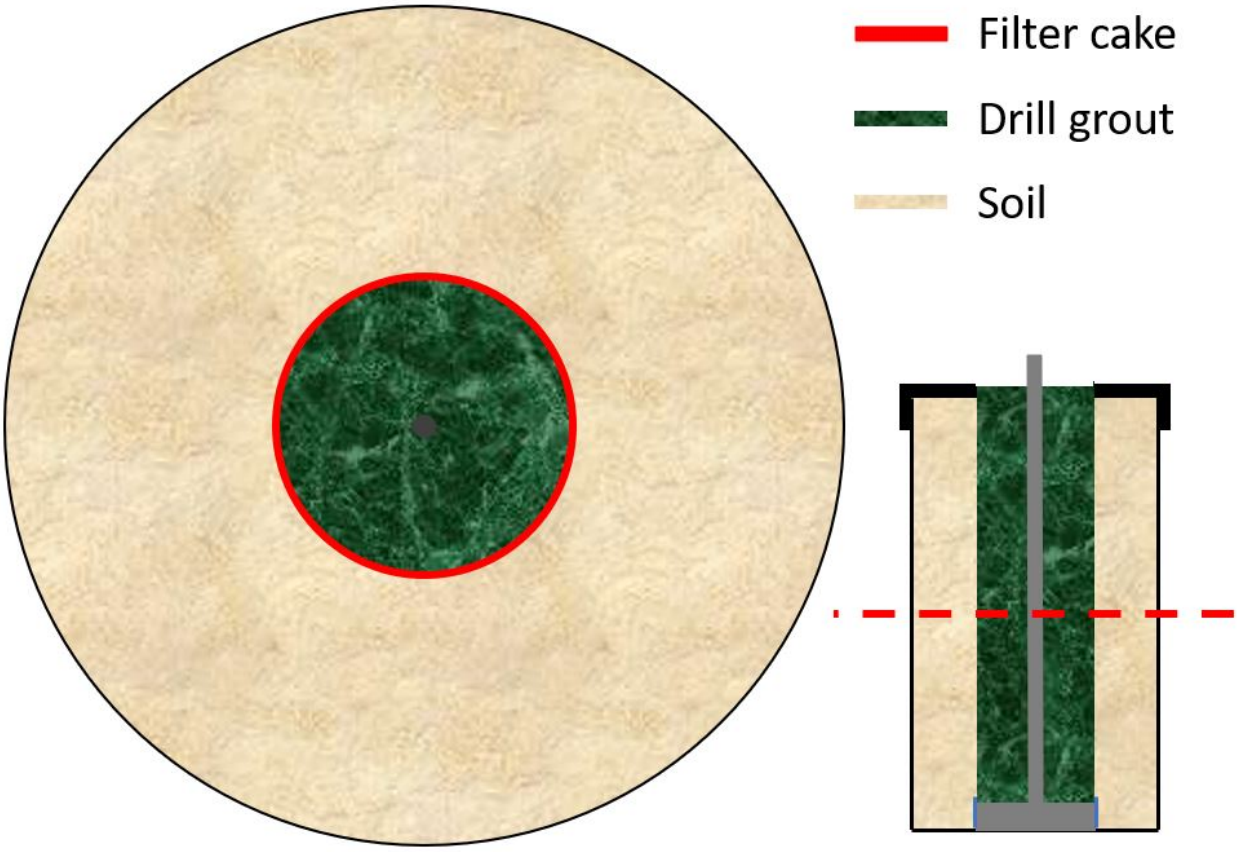

Figure 21: Horizontal cross sectional area of the sample

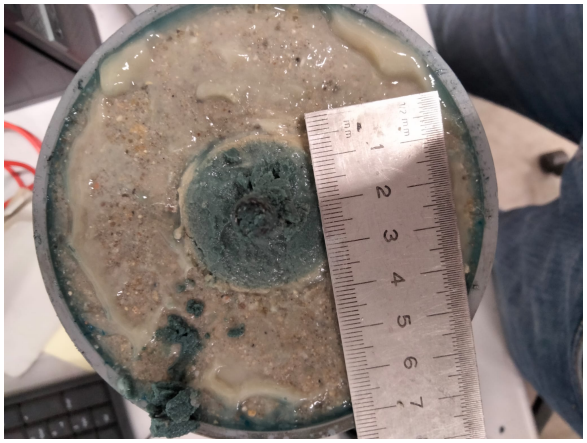

(a) Cross section of the sample before the pull out phase. This sample was used for test 1 4.

(b) Cross section of a sample where a filter cake has been formed by pressurising drilling fluid, but no drill-grout has been cast afterwards. This was the sample used for test 3.

Figure 22: Top view of the samples

force will decrease linear until the test ends.

The pull out force of test 1, sample 1 and 4 do have a "bottom peak" so to say. In other words, after the

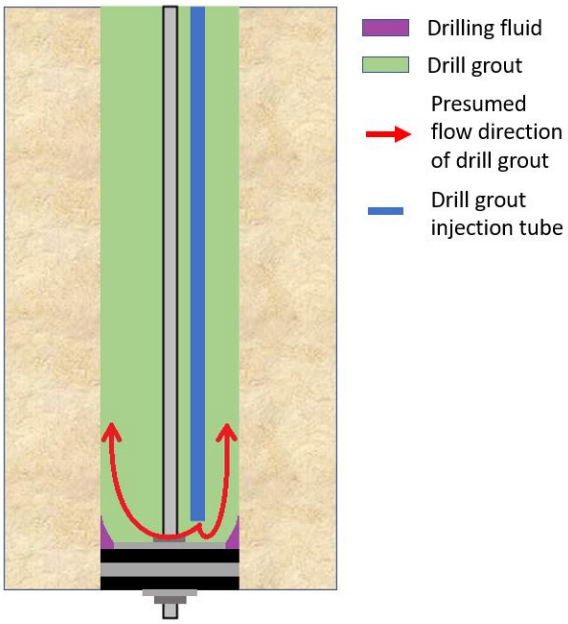

(a) Cross section of the sample before the pull out phase. This sample was used for test 1 4.

(b) A picture of the drill grout column after it was pulled out of the sample. A build up of sand particles can be seen at the bottom part of the column.

Figure 23

pull out force decreases, it reaches a bottom and starts increasing after that. In here, as can be seen in figure 49, the overall trend from the peak to the end of the test is decreasing. The difference from other tests is that the pull out friction decreases a lot faster because the friction of the system is lower than average. After some time, the bottom cylinder of the pull out thread makes contact with the soil again which causes the friction to increase.
Sample 3 of test 1 and 4 show an increasing pull out force to the end of the test. Though, the start of a peak in the first part of the test can be seen also. In these tests it is thought that the accumulation of sand particles causes the shear stress to increase. Because of this, the friction of the system will increase endlessly.
Test 4, sample 2 and 4 do show the expected trend but deviate a little from it. As can be seen in sample 2, the peak of the pull out force should be somewhere around - 50 mm of displacement. This is because the slope gradient decreases which should result in a peak. But, the pull out force keeps increasing untill the peak is reached at the displacement of -170 mm.
The same can be said for sample 4, but in this test a peak is reached only the decrease of pull out force is too low compared to the other tests. For both samples the explanation is the build up of soil particles or an increase of friction caused by the bottom cylinder scraping the borehole wall.

4.2.3 Polynomial fit

The plotted results from every test show large and small oscillations from a general trend. These oscillations can be logically explained and thus it has be decided that a polynomial fit of every data set will be plotted. These fits are an estimate of the average trend line of the data set and will then be analysed instead of the true data set. A polynomial fit of a data set is composed of a general formula: $y = a_0 + a_1x + ... + a_kx^k$, where k is the order of the polynomial fit. Every order until the 6th order of polynomial fits have been calculated and plotted and are shown in the appendix. Figure 46 shows a 2nd order polynomial fit, figure 47 shows a 3rd order polynomial fit, figure 48 shows a 4th order polynomial fit, figure 49 shows a 5th order polynomial fit and figure 50 shows a 6th order polynomial fit of the results. The 2nd order polynomial fit is too divergent from the general trend of the graphs (fig 24a). It was chosen to fix the start of the fit at x,y = 0,0 since the start of

the fit lines would be too high. The fits would sometimes start higher than 100 N. The 3rd order polynomial looks less divergent, but as its examined closer it can be seen that the start of the fit is very unrealistic (fig 24b. When the start of the fits were fixed at zero, the lines would be too divergent from the trend of the real data.

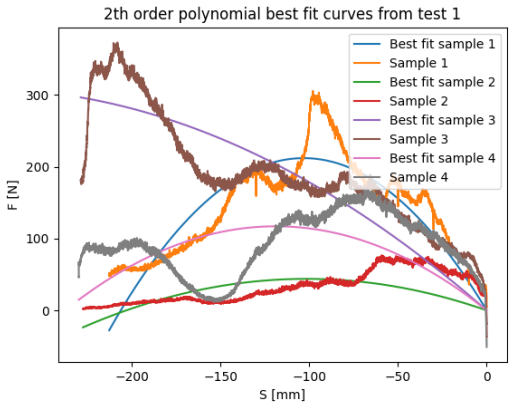

(a) Results from test 1 with a 2nd order polynomial best fit

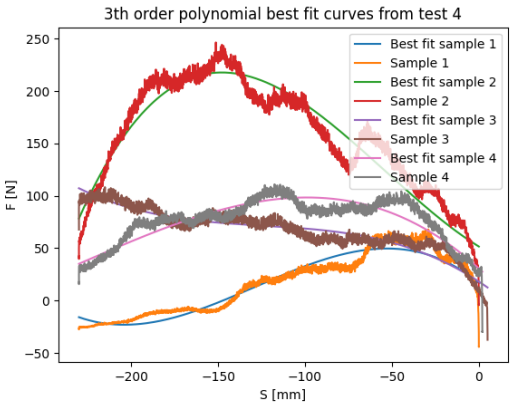

(b) Results from test 4 with a 3rd order polynomial best fit

Figure 24: 2nd and 3rd order polynomial best fit

The start of the fit is very different in each test and can be up to 100 N which is very unrealistic. The 4th order follows the trend of the graphs just enough that it ignores the minor and larger oscillations (fig 28a). The 5th and 6th order fits follow the graph too well which decreases the practical use of the computations (fig 25). This is the reason that the 4th order polynomial best fit of all the generated plots is used to analyse the results. Test 3 is a test done without drill grout to find the friction caused by the system itself. The friction values of

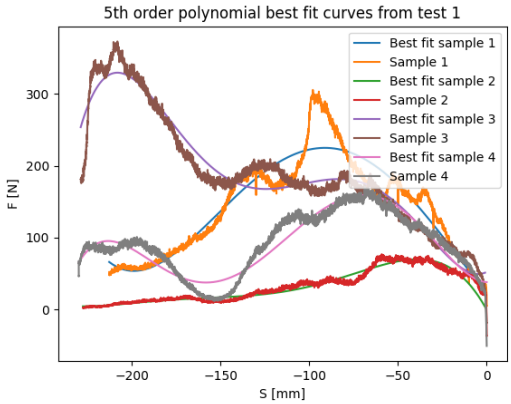

(a) Results from test 1 with a 5th order polynomial best fit

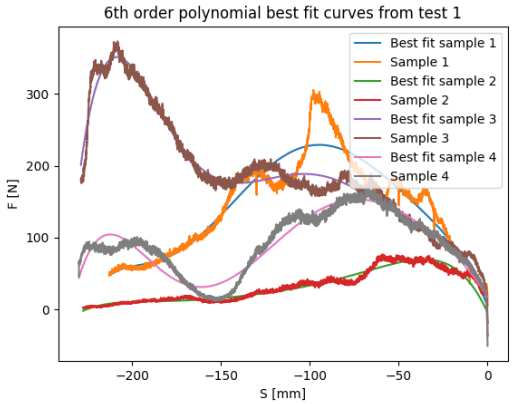

(b) Results from test 1 with a 6th order polynomial best fit

Figure 25: 5th and 6th order polynomial best fit

the system were assessed and their maximum values were subtracted from the pull out forces measured in tests 1, 2 and 4.

4.2.4 Normalisation

For the normalisation of the acquired data, the following formula was used: $\tau = \frac{F}{A'}$, where A' is the frictional surface that is located in between the drill grout column and the soil column (see figure 26). A' is calculated with the following equation: $A' = \pi * D * (L - S_i)$, where D is the diameter of the drill grout column, L is the total length of the soil body and S_i is the displacement of the drill grout column at a certain interval of the test.

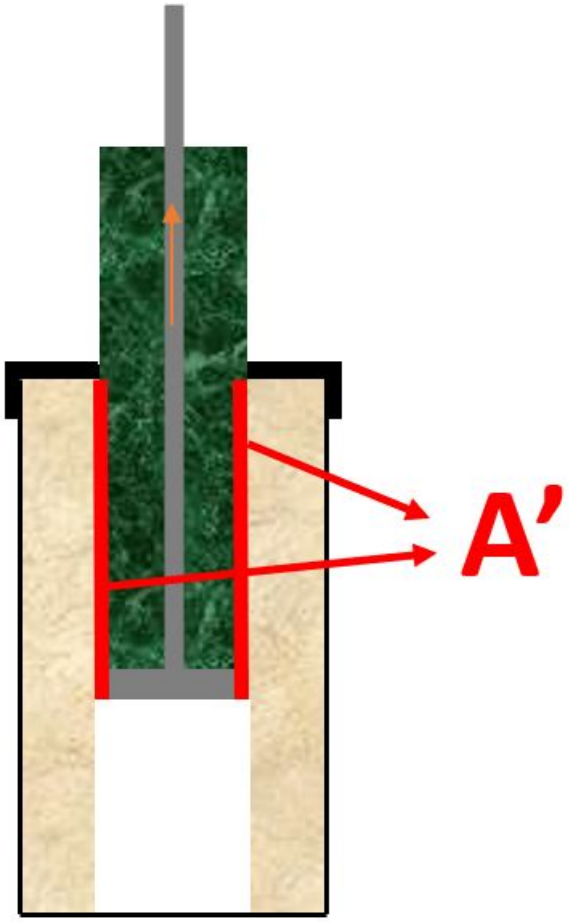

Figure 26: The red line shows a cross section of the frictional area that should represent A' at a certain moment during the test.

Two of the most representative normalisation graphs are shown in figure 27. 8 out of 12 graphs follow the trend seen in figure 27 trend clearly. Because the drill grout column is being pulled out of the soil column, the frictional surface area decreases until the drill grout column is pulled out of the soil column entirely. When the pulling force is entirely dependent on the friction between the drill grout and soil, The normalised shear stress (τ) should remain constant over the course of the test. As can be seen in figure 42, 43, 43 and 45 from the appendix, this is never the case. For a few tests such as sample 1 of test 1, sample 1, 2 and 4 of test 3 and sample 4 of test 4 an argument could be made that τ was constant after some part of the test, but the high fluctuations in the calculated shear stress makes this argument very hard to support. Also, do note that test 3 was the test done without drill grout. So here there should be no friction apart from the DPIA itself. Decreasing the numerator while keeping the denominator constant should give a linear increase in τ. Apart from test 3, sample 3, this result is not represented in the graphs. This could be explained by the fact that the sand particles that got scraped off the sand column were able to float loosely in the bentonite fluid, in contrast to the other tests with drill grout where the sand particles were stuck in between the drill grout and sand column.

The fact that most other results show an increasing shear stress when normalising the results, indicate that the friction is mostly induced by factors other than the friction between the drill grout and soil. This assumption is made because of the fact that there is no theory to support any increase in frictional behaviour of grout over this amount of displacement. However, it is generally accepted that this behaviour occurs in soils such as sand. This phenomenon is called "slide and slip" behaviour and is often seen in shear tests with sand samples. "slide and slip" is a term used to describe the case where particles interlock due to their displacement towards each other. This interlocking increases the friction angle of the soil particles. When the particles either break due to failure, or get pushed over each other the required force for displacement suddenly drops which causes a sliding motion of the sand. After this, the particles will interlock again which causes the soil to slip. This phenomenon

could explain the high oscillations in shear stress that are shown in the graphs.

It is concluded that the normalisation shows that the stress is mainly caused by the DPIA itself instead of the friction between drill grout and the soil. The DPIA could create a build up of sand particles on the bottom of the drill grout column which increases the friction significantly. The argument for this is the ever increasing shear stress which show that the frictional force must be induced by something other than the contact area between drill grout and soil.

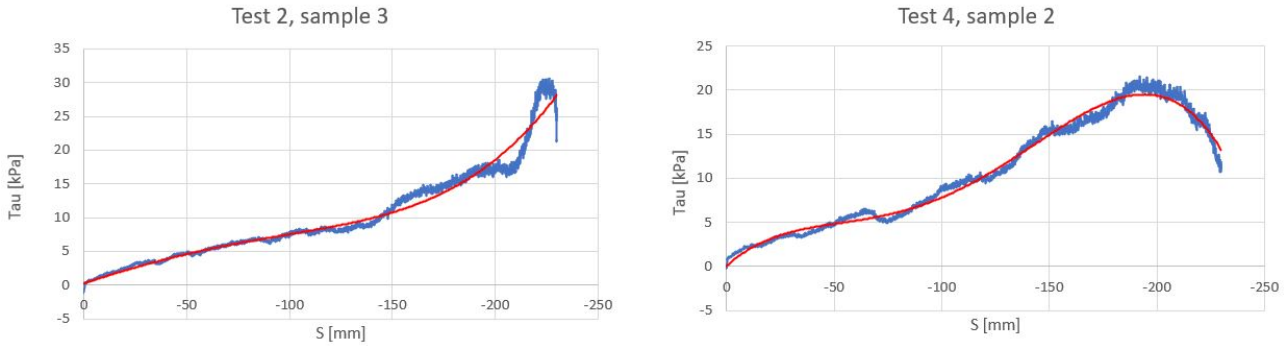

Figure 27: Normalisation of test 1

4.2.5 Correction for the friction of the system

As was mentioned before in the previous paragraph a separate test was done to measure the friction of the system. This friction will have to be accounted for and subtracted from the test results. The samples made for test 3 were made without the casting of drill grout. This means that only step 1 to 12 from figure 18 were done to make the samples. Before the pull out phase was initiated, the bentonite was poured out of the sample. This left only a filter cake in a hollow cylinder. Just like in every other test, 4 samples were made so 4 data sets were obtained. A picture of the sample is shown in figure 22b. The results of the tests with a best fit curve are shown in figure 28a. From these curves, a maximum curve and a minimum curve was created. This was done by comparing the measured pull out force of every sample at the same position. The maximum and minimum pull out force were plotted separately to give figure 28b. In this figure the maximum and minimal frictional curves are shown. As can be seen, the peak of the curves are reached after a similar amount of displacement. The difference of the maximum of these peaks is 48.7 Newtons. Every result from test 1, 2 and 4 will have to be corrected for the maximum and minimum frictional values measured in test 3. This means that the friction between the drill-grout and the soil is in between 86.7 N and 38.0 N smaller than is actually measured.

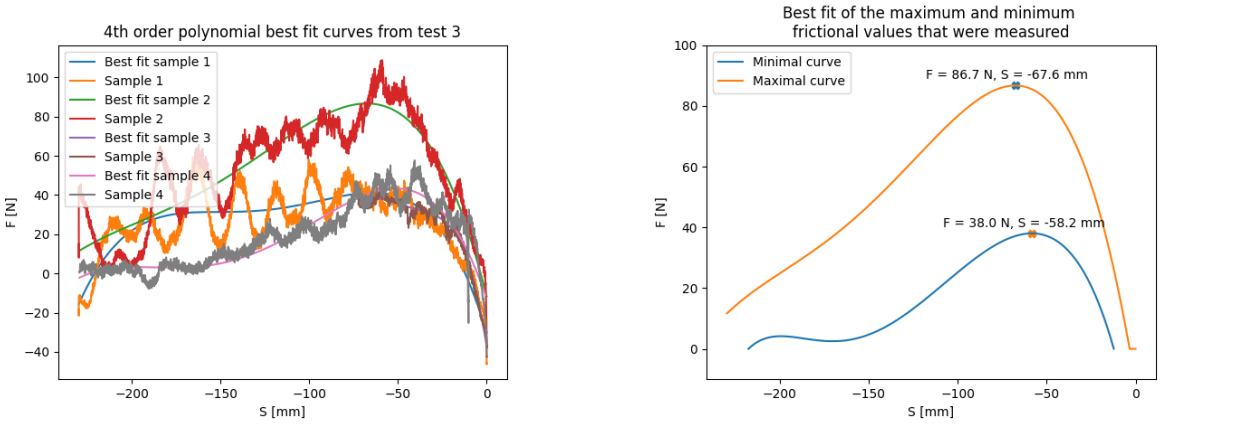

(a) Results from test 3 with a 4th order polynomial best fit

(b) Minimum and maximum curve obtained from the best fit data set from test 3 shown in figure 28

Figure 28: Test 3 minimum and maximum curves

4.2.6 Test 1, 2 and 4

The results of test 1, 2 and 4 are shown in figure 29b and 29a. Because the samples of test 2 had not hardened sufficiently, test 2 is left out of consideration for calculating the friction between drill-grout and soil. Though, it is good to notice that the pull out force of test 2 is within the domain of test 1 and 4. This indicates that the strength of the drill-grout does not influence the friction between drill-grout and soil.
Leaving test 2 out of consideration, Figure 30b and figure 30a are given. From these two figures, Figure 30a shows that in half of the samples the friction could be between 0 and 50 Newton. A boxplot was made to asses the outliers, average and minimum and maximum friction values.

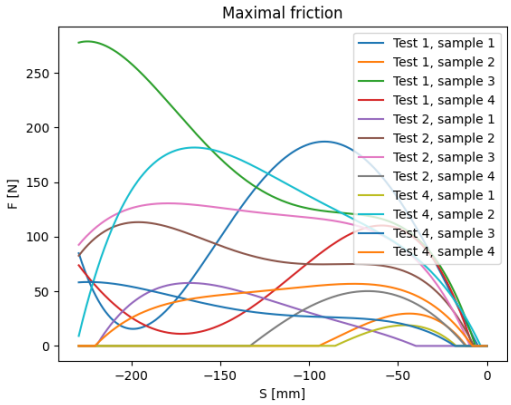

(a) Measured pulling force corrected for the minimal average friction of the system.

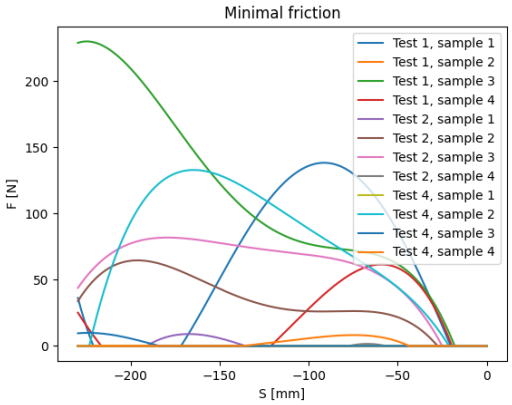

(b) Measured pulling force corrected for the maximal average friction of the system.

Figure 29: Top view of the samples

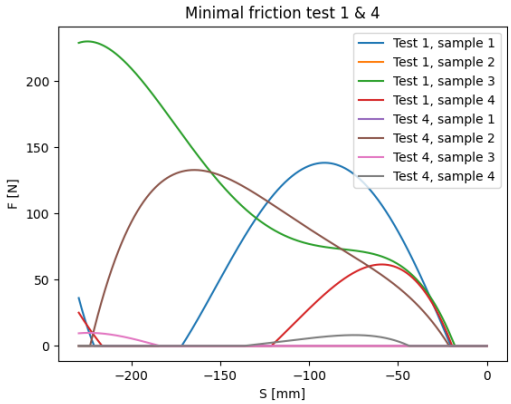

(a) Measured pulling force corrected for the minimal average friction of the system.

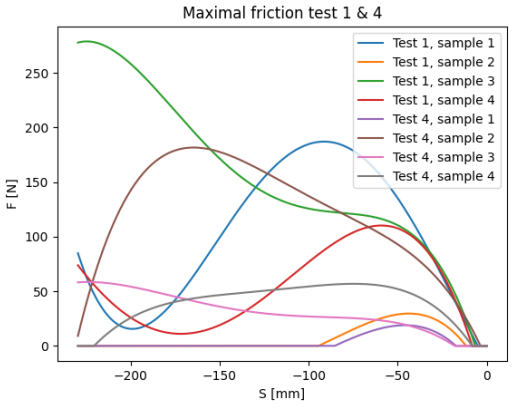

(b) Measured pulling force corrected for the maximal average friction of the system.

Figure 30: Top view of the samples

Figure 31 shows a more coherent representation of Figure 30b and Figure 30a. For these values, the maximum of every graph was taken. It could be said that the total domain of the results lies within 0 to 300 Newton while half of the results . 0 Newton is found when the lowest friction measured is considered and the highest friction of the system accounted is for. 300 Newton is found when the highest measured friction is considered and the lowest friction of the system is accounted for. The box plot shows that the higher values could be considered more as outliers than the lower values since the median lies very close to the lower quartile and the lowest value.

H. Ostermayer and F. Scheele (1978) have done research about the friction of ground anchors in non cohesive soils and they have found that the skin friction between cement and non cohesive soils are in between 100 kPa and 1300 kPa (see figure 32) [15]. The soil used in the research for this thesis has a density that could

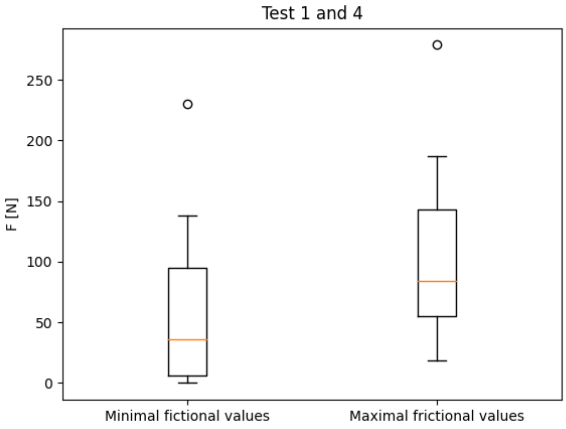

Figure 31: Boxplot of test 1 and 4

be refered as medium at the least. The samples were (show soil grading) created with two different types of sand and compacted by shaking the container for multiple times while it was being filled. This indicates that the results should be compared to the skin friction that was measured between grout and medium dense sand which gives a range in between 300 kPa and 1300 kPa.
H. Ostermayer and F. Scheele (1978) have used cement which creates a much stronger bond with sand than drill grout. It can't be said how much stronger the adhesive strength between cement and sand is because the adhesive strength between drill grout and sand has not been tested yet. Drill gout is the mix of more than 97 % of weak cements and some bentonite and other additives to keep the viscosity of the mixture such that it can be easily pumped and poured into the boreholes. considering this information one would expect drill grout to have a lower skin friction than the grout anchors used by H. Ostermayer and F. Scheele, but not by a factor of 1000. All of the points noted above concludes that the filter cake prevented any chemical bonds to have formed between the drill grout and the sand particles.

Although the data obtained from the DPIA method is within a range of 300 N, It can be said that this range is relatively small compared to range shown in figure 32. Based on this, two things can be said: 1. The range of the results obtained by the DPIA tests are relatively small compared to tests done with normal grout. At first sight it seems that the range of the data is very wide and that there could be something wrong with the test method or measuring equipment. But, when the results are compared to other frictional tests done with grout, it is concluded that a range of 300 N is actually relatively small and that the results are very much reliable and use able to answer the research questions. 2. The friction that is measured is mainly caused by either the viscosity of the filter cake or the friction between the bottom cylinder of the pull out thread and the soil. Another point to note is that the friction keeps rising while the frictional area decreases. This is to be expected in the first 10 millimetres, but after that it is expected that the friction should decrease since the frictional area decreases. This is an argument as to why the measured friction is expected to be mainly caused by the accumulation of sand in between the bottom cylinder and the drill grout column.

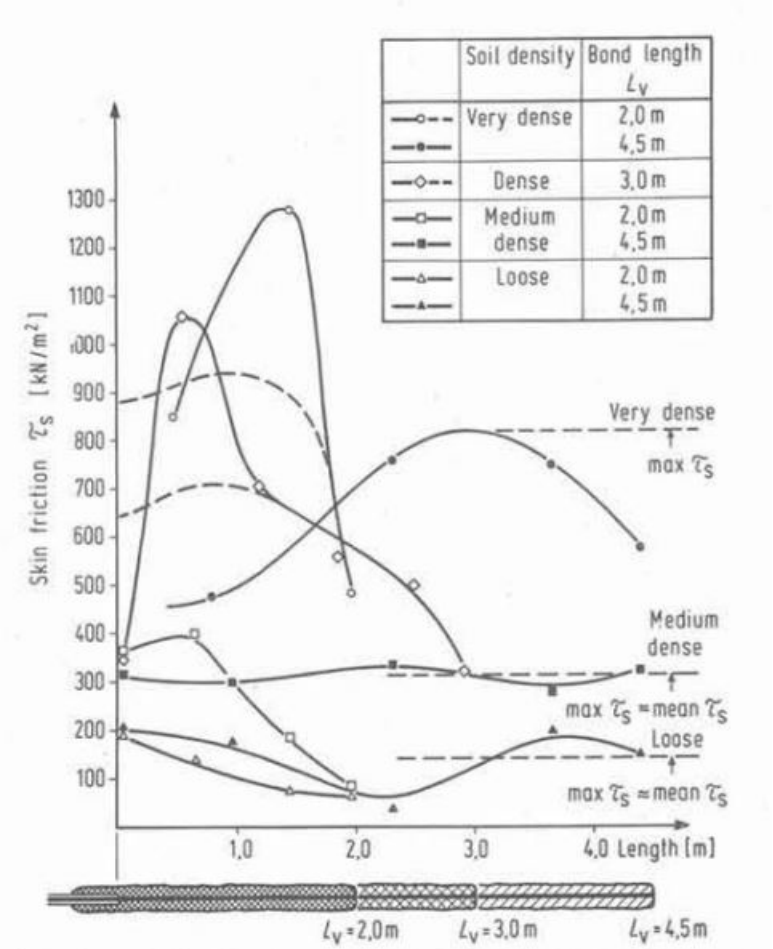

Fig. 9. — **Distribution of long-term skin friction τ_s at ultimate load in relation to bond length L_v and soil density.**
Grouted bodies (d_o = 9.1 — 12.6 cm) in gravelly sand.

Figure 32: This figure shows the results gained by H. Ostermayer and F. Scheele (1978)[15]

5 Calculations

5.1 Grout to soil interface friction calculation

The minimum and maximum pull out forces are shown in table 6. The area of the drill grout column is 0.0339 m^2. The area and pull out forces can be used to calculate a shear stress by the hand of equation 4 or 5.

$$\tau = \frac{F}{A} \tag{4}$$

Where :
F, the pulling force corrected for the friction of the system
A, the area of the drill grout column

$$\tau' = \frac{F}{A'} \tag{5}$$

Where :
A', the area of the drill grout column at the point of the maximum pull out force

When using equation 4, the shear stress is calculated by using the total surface area of the soil column. When using equation 5, the shear stress is calculated by using the reduced area due to the displacement of the drillgrout column. Because of this, the results calculated with equation 4 are expected to be lower than in practice. Because the friction of the system was measured to be in between 86.7 N and 38.0 N, a margin of error had to be considered. Using equation 5 it was found that the shear force of the system was in between 2.0 and 0.9 kPa (the relative area was taken into consideration). These were subtracted from the calculated shear stresses to obtain a minimal and maximal shear stress value. The resulting shear stresses of both methods are shown in table 3. Because the results of test 2 were not reliable enough and during test 3 no drillgrout was used, only the results of test 1 and 4 are shown.

Test	Sample	τ' min	τ' max	τ min	τ max
1	1	12.2	13.3	4.08	5.52
1	2	0.9	2.0	0.00	0.87
1	3	54.5	55.6	6.78	8.22
1	4	14.8	15.9	1.82	3.25
4	1	0.4	1.5	0.00	0.56
4	2	19.6	20.7	3.92	5.36
4	3	17.9	19.0	0.29	1.73
4	4	6.3	7.4	0.24	1.68

Table 3: The calculated shear stresses from equation 4 and 5.

A combination of equation 4 and 5 is also used. In this calculation, the maximal friction force was considered from a non normalised graph. Afterwards, the shear stress was calculated by using the normalised surface area. This method considers a realistic peak friction force, while also considering the realistic frictional area. These results can be seen in table 4.

Test	Sample	Tau min [kPa]	Tau max [kPa]	Average tau [kPa]
1	1	6.160	8.326	7.243
1	2	0.000	1.041	0.520
1	3	40.281	48.800	44.541
1	4	2.324	4.160	3.242
4	1	0.000	0.673	0.337
4	2	10.027	13.697	11.862
4	3	1.702	10.083	5.892
4	4	0.334	2.316	1.325

Table 4: Semi normalised shearing forces from test 1 and 4

A maximum and minimum shearing force created by the friction between the drill-grout and soil in the sample was calculated and is shown in table 4. An average shearing force was also calculated. All the results

from test 1 and 4 are shown in figure 33. Figure 33a shows a boxplot of the maximum and minimum shear forces. Figure 33b shows al the average shear forces of test 1 and 4. Since the shear force of 44.5 kPa is an outlier it is removed. This gives figure 33c. As the displacement of the sample becomes higher, the bottom cylinder of the pull out column comes closer to the lid of the container. The accumulation of sand on the bottom cylinder will now create a greater shearing force. This force could distort the data, so only the first half of the test will be considered. This is the part where the surface area is in between 34000 mm^2 and 17500 mm^2. This leaves the three data points shown in figure 33d.

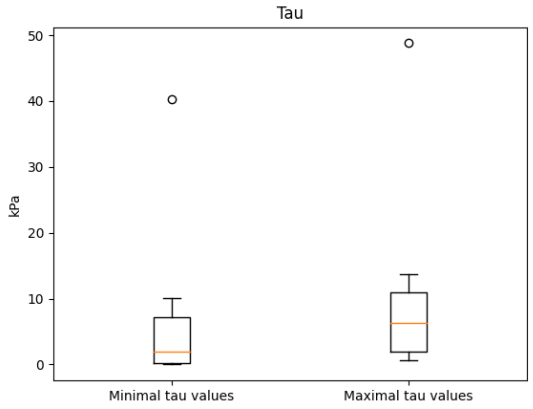

(a) Boxplot of the shear force calculated from test 1 and 4

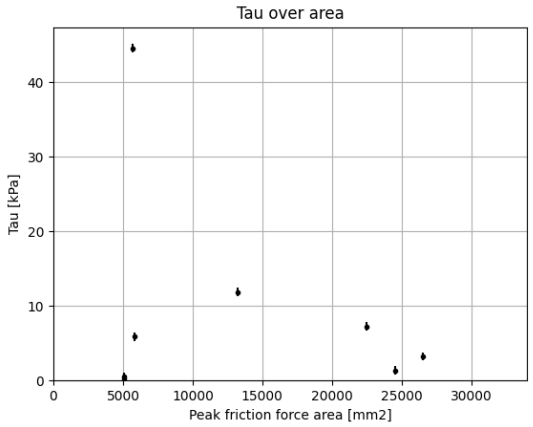

(b) The shear force compared to the frictional area at the maximum pull out force

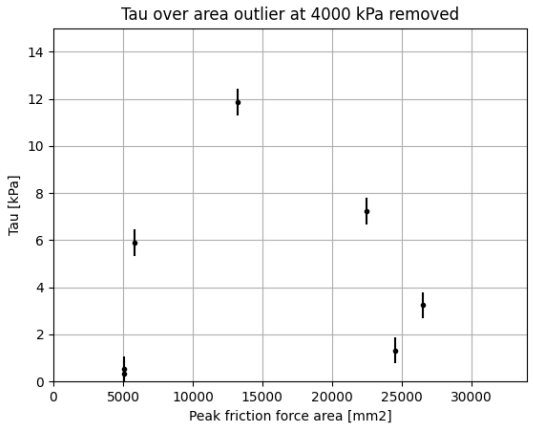

(c) The shear force compared to the frictional area at the maximum pull out force. The outlier of 44.5 kPa is removed.

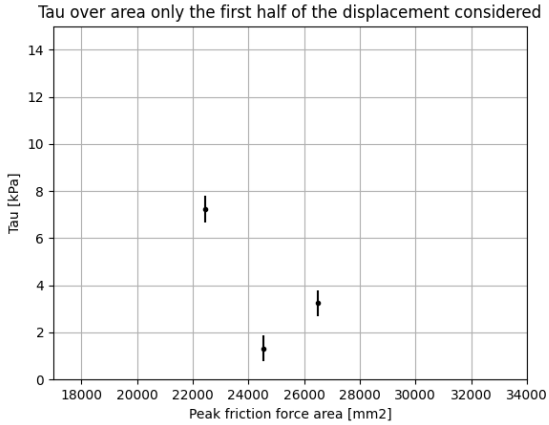

(d) The shear force compared to the frictional area at the maximum pull out force. The outlier of 44.5 kPa is removed and only the first half of the total surface area is considered.

Figure 33: Test results from test 1 and 4

R. Tognon et. al have done research about the friction between sand and PE [21]. They found that the shear stress created by the frictio between PE and sand lies in between 10 kPa and 150 kPa 34.

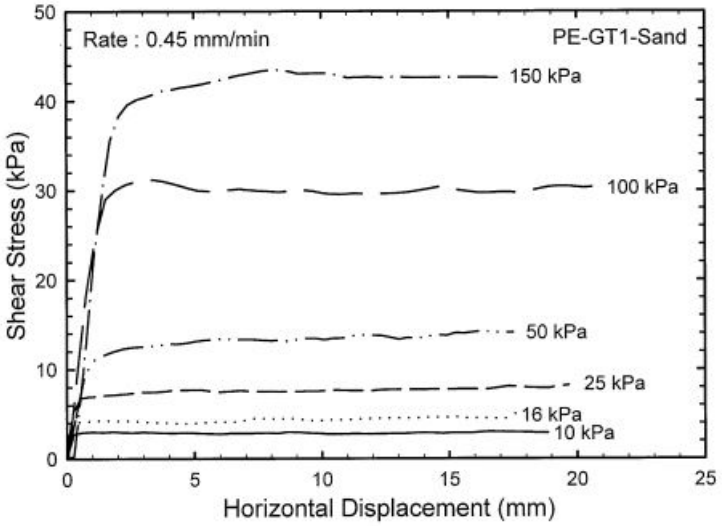

Fig. 6. Shear behaviour of unlubricated PE-GT1-Sand interface.

Figure 34: Shear behaviour of unlubricated PE-GT1-Sand interface [21]

Considering these results, it can be said that the friction between sand and drillgrout is considerably lower than the friction between sand and PE.

5.2 Design of heat transportation lines

5.2.1 Friction factor comparison

In the field there is one generally used method for the thermal expansion calculations of heat transportation pipes. These calculation methods have been developed by the constructors of the pipes and have later been added to the NEN 3650-1 as a standard. A very common used brand for heat transportation pipes is Prinspipe. Most of the calculations that can be found in the NEN-3650-1 considering heat transportation lines are derived from the knowledge provided by Prinspipe. One must note that all of these calculations are regarding open trench method. This is because no heat transportation lines have been constructed by the hand of trench less methods yet.

Prinspipe uses the following formula to calculate the frictional force between the soil and the PE pipe:

$$F_r = \mu * (G + \gamma * D * (2 * H + K_d * (H + D/2) * (\pi - 2))) \tag{6}$$

Where:
F_r, the friction force [N/m];
μ, the friction factor [0.5];
γ, the volumetric weight of the soil;
K_d, the pressure coefficient in resting position;
G, The weight of the medium pipe + water [N/m];
D, the outer diameter of the pipe [m];
H, the depth of the pipe [m];

In the prinspipe manual is an example calculation using equation 6 and general soil values. They show that a PE pipe is buried in sand has an approximate friction force of F_r is 5063 N/m[**PRINSPIPE2010TechnischeDocumentatie**]. It was tried to back calculate the friction factor by using the results of R. Tognon et. al. For this, one must calculate F_r and then solve for μ. A way to calculate F_r is by using the reasoning that the surface of the pipe is calculated by multiplying the circumference of the pipe with the length of the pipe. In the example shown by Prinspipe a pipe with a diameter of 250 mm was used. This pipe would have a circumference of 1.02 meter. When the friction force is back calculated by using the lowest shear stress found by Tognon, the friction force would become at least 2 times as large as the friction force found by Prinspipe ($F_r = 10[kN/m^2]/1.02[m] \approx 10[kN/m]$). This concludes that back calculating F_r by using the circumference and the shear stress is not correct. It is better to compare both shear stresses and deduct an approximate friction factor.

As shown in figure 33 the frictional shear stress between drillgrout and sand is in between 3.2 kPa and 7.2 kPa while the frictional shear stress between sand and PE is in between 10 kPa and 150 kPa. This means that the friction factor μ must be significantly smaller than 0.5 for drillgrout to sand contact. Since there is such a large spread in the results of Tognon et. al, it is not realistic to approximate a friction factor for the drillgrout. However, one can conclude that any pipe constructed by the hand of HDD experiences a much smaller friction force than a pipe constructed by the hand of open trench method. The only thing to conclude regarding further calculations is that the upper bound of the friction factor is 0.5.

5.2.2 Normal force due to pressure build up

$$\sigma_{ax} = \alpha_g * E(t_2) * \Delta t \tag{7}$$

Where σ_{ax} is the axial stress generated by hindered displacement $[N/mm^2]$, t_1 is the temperature at the time of construction $[^\circ C]$ and t_2 is the medium temperature at time of operation $[^\circ C]$, α_g is the average linear expansion coefficient between t_1 and t_2 $[(mm/mm)K^{-1}]$, $E(t_2)$ is the elasticity modulus at temperature t_2 $[N/mm^2]$ and Δt is the temperature difference of the medium liquid at the time of construction and operation. According to the prinspipe manual, σ_{ax} is the maximum allowable axial stress in the pipe. [**PRINSPIPE2010TechnischeDocumentatie**][14].

The force generated by the medium pipe is then calculated by using the crossectional surface area of the metal pipe.

$$N(t_2) = \sigma_{ax} * A \tag{8}$$

Where $N(t_2)$ is the generated normal force at temperature t2 in the metal medium pipe and A is the crossectional surface area of the metal medium pipe. Combining equation 7 and 8 gives:

$$N(t_2) = \alpha_g * E(t_2) * \Delta t * A \tag{9}$$

When $N(t_2)$ is equal to the friction force (F_r) there is a change of buckling since the pipe cannot expand over its length axis. A 20/90 diameter pipe Prinspipe has the following properties:

- $\alpha_g = 1.2 * 10^{-5}[(m/m)/K]$
- $E(t_2) = 2.1 * 10^{11}[N/m^2]$
- $A = 4.18 * 10^{-4}[m^2]$

To investigate the effect of the maximum temperature change (Δt) realistically possible, a Δt of 80 K is considered. Then the normal force developed due to temperature change during prevented expansion will be:

$$N(t_2) = \alpha_g * E(t_2) * \Delta t * A = 1.2 * 10^{-5}[(m/m)/K] * 2.1 * 10^{11}[N/m^2] * 80[K] * 4.18 * 10^{-4}[m^2] = 93.5kN \tag{10}$$

When the frictional force between the drill grout and soil is greater than $N(t_2)$, expansion over the longitudinal axis will be prevented. Since the pipe will never be laid completely straight, there will be "weaker" points at the curvatures whereto the expansion will propagate. This phenomenon is called buckling.

To prevent buckling, the length of the pipe must be kept to such a length that the build up of soil friction will not exceed 93.5 kN. This calculation is done by the hand of the following formula:

$$L_{max} = \frac{N(t_2)}{F_r} \tag{11}$$

As explained in the previous paragraph, F_r can be calculated by using formula 6. To use this equation, a certain set of parameters have to be set. To make sure that an upper bound of the friction parameters is chosen, general parameters of sand are used. Taking a DN150/250 from the prinspipe manual concludes the following parameters:

μ, [0.5];
γ, 19 000 $[N/m^3]$;
K_d, 0.463;
H, 10 [m];

The results can be seen in the table below.

Nominal diameter steel pipe	[DN]	20	25	32	40	50	65	80	100	125	150	200	250	300	350	400	500	600
Diameter outer PE pipe	D. [mm]	90	90	110	110	125	140	160	200	225	250	315	400	450	500	520	630	800
Weight	[kg/m]	2.9	3.4	3.9	4.3	5.7	7.2	9.8	13.2	16.2	21	31.2	45.2	58.6	66.6	84.4	114	149.3
Water content	[l/m]	0.4	0.6	1.1	1.5	2.3	3.9	5.4	9	13.8	20.2	34.7	54.3	76.8	93.2	121.8	192.8	278.8
G	N/m	32.373	39.24	49.05	56.898	78.48	108.891	149.112	217.782	294.3	404.172	646.479	976.095	1328.274	1567.638	2022.822	3009.708	4199.661
D	m	0.117	0.117	0.143	0.143	0.1625	0.182	0.208	0.26	0.2925	0.325	0.4095	0.52	0.585	0.65	0.676	0.819	1.04
Fr	N/m	28155.47	28158.9	34426.32	34430.2	39140.14	43856.37	50147.47	62733.98	70624.24	78536.48	99111.45	126078	142047.9	157983	164542.7	199923.3	254636.8

Table 5

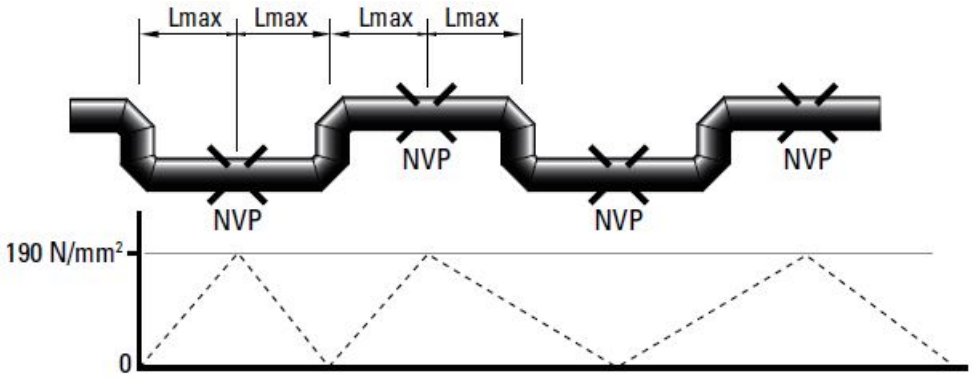

Figure 35: A figure from the Prinspipe manual that shows the pressure build up due to thermal expansion.

The larger the diameter of the pipe, the higher the friction per length unit of the pipe will become. Regarding the smallest diameter available, the results from table 5 show that the maximum length of a pipe segment in between two expansion loops can be $2^{*}L_{max}$ (figure 35) which is smaller than 6.64 meters.

6 Conclusion

The first thing that must be concluded is that based on this research method, providing these results, it is not possible to make a realistic buckling calculation. Too many parameters that can affect the chance of bucklink cannot be realistically derived nor calculated. Two of these parameters would be the friction angle and the E-modulus. The friction angle cannot be derived since the tests were done without a normal force. To find the E-modulus, a whole different test needs to be done all together. Since this is out of the scope of this research, a conclusion will be drawn out of the results that were found with the DPIA method.

While drilling, the fluid pressure in the borehole creates a filter cake in between the soil and the drillgrout which reduces the friction between those two significantly. However, this is only tested during negligible soil stresses. Although an accurate method to calculate a friction factor for this situation has not been found yet, it is possible to compare the friction between drillgrout and sand with the sand to PE interface. Using figure 34 it is concluded that the friction between drillgrout and sand is much lower than the friction between sand and PE, thus the friction factor between drillgrout and sand is much lower than that of sand and PE which is 0.5 according to NEN 3650-1 [14]. However, the real friction that can be found between the drillgrout and soil at the depth of a pipe laid by the hand of HDD is dependent on the soil stresses and the diameter of the of the borehole also. Because those are both considerably larger it is found that the friction that has to be accounted for in the situation of a pipe laid by the hand of HDD with drillgrout is much larger than the friction for a pipe laid by open trench method.

The maximal shear stress that can occur between drill-grout and soil (τ_{ds}) is measured to be 0.0 $[kN/m^2]$ $< \tau_{ds} <$ 13.7 $[kN/m^2]$. Even though this is much lower than the shear stress found between PE and sand, it is still recommended to account for the friction between drill-grout and soil due to the strength of the metal medium pipe which is used in heat transportation pipes. Also, this test was done with a neglible diameter change troughout the borehole. In a real situation, the borehole diameter will vary over the length of the borehole increasing the friction significantly. The expansion forces of the pipe will create a sufficient force to

either tear apart the insulation PUR layer, or to create a buckling effect in the pipe all together.

7 Experience and recommendations

The construction of the DPIA and the research method has cost a lot of time and effort that is not described in this report. Almost every part of the DPIA had to be adjusted at least once. When one part would be adjusted, other parts would have to be adjusted too and sometimes even the whole application would have to be rethought of. In this section the experiences are summarised shortly to try to give an understanding of the development steps that would have to be made to create the DPIA and the research method. After this some recommendations are given for anyone who would like to use this research method.

7.1 Experience

From the start PVC was chosen as the best material for the DPIA. This is because it is relatively cheap and easy to come by. In every local construction shop one is able to obtain PVC sewer pipes in different diameters. Also, it is possible to buy accessories like screwable caps end caps. Thereby, these different parts can be glued on to each other. The downside of the PVC material was that it has a low strength and is prone to degradation due to the friction with sand. Also, because of its low strength, sand grains would get pushed into he PVC which increased the amount of friction between different parts significantly. There were two parts that could be fixed and removed by screwing and this needed a significant amount of force. Sometimes even tools would have to be used. This was very problematic because the samples should be disturbed as little as possible. Based on quality of the DPIA alone, stainless steel is the better material.

When the first prototype was finished, it was constructed without a stand pipe and had no outer column extension. When the drilling fluid was pressurized, fluids were able to flow out of two tiny holes made in the cap of the DPIA. Without these holes it would have been impossible for fluid to flow trough the soil and thus it would've been impossible for a filter cake to form. During the first tests, there would always be some kind of soil collapse. The cause of these collapses were thought to be liquefaction and a vertical pressure exerted on the soil column by the bentonite that was found to be in between the outer column cap and the soil (see figure 36). This problem was solved by installing a standpipe so that the fluid pressure was always higher than the pore pressure in the soil.
Because the standpipe was so much bigger than the holes in the cap of the DPIA, much more fluid was now able to flow out of the DPIA. Because of this, additional bentonite fluid will need to be in the inner column so that the inner column remained fully filled with bentonite fluid. This was done by extending the inner column with a pipe that could be screwed on top of the outer column cap. The extension part would have to be removable so that the DPIA would still be able to fit in an oven.
When all these parts were made, it seemed that the small size of the DPIA caused the margin of error to be small also. Everything from the sample making to the testing phase had to be perfect for a realistic data set. This is why a larger prototype was also build. This prototype had a 1 meter length and a diameter of 0.5 meter. After a couple of samples were made it was concluded that this prototype was not suited for this thesis since it was too heavy, required too much soil and it did not fit in any oven. Besides that it made the sample making process possibly harder, the samples would have to hydrate for at least 28 days which would cause the time needed for the research to be too long. Nevertheless, the construction of this prototype was not a complete waste of time because its size made it able for me to better understand the soil collapse.

Another difficulty was to create a straight pull out threat (figure 15b) that could be used for pulling out the sample. The screwing thread was either not completely straight by itself, or the fixation of the pull out thread caused it to be not entirely straight (see figure 37). It is thought that the rubber parts in the bottom could be compressed unevenly during the fixation of the pull out thread which caused the axis of the pull out thread to deviate from the drill grout axis. This could cause the pull out thread to be pulled into the soil which could cause non axial loading. Because the margin of error is so small, even the smallest of deviations could cause a higher friction to be measured.

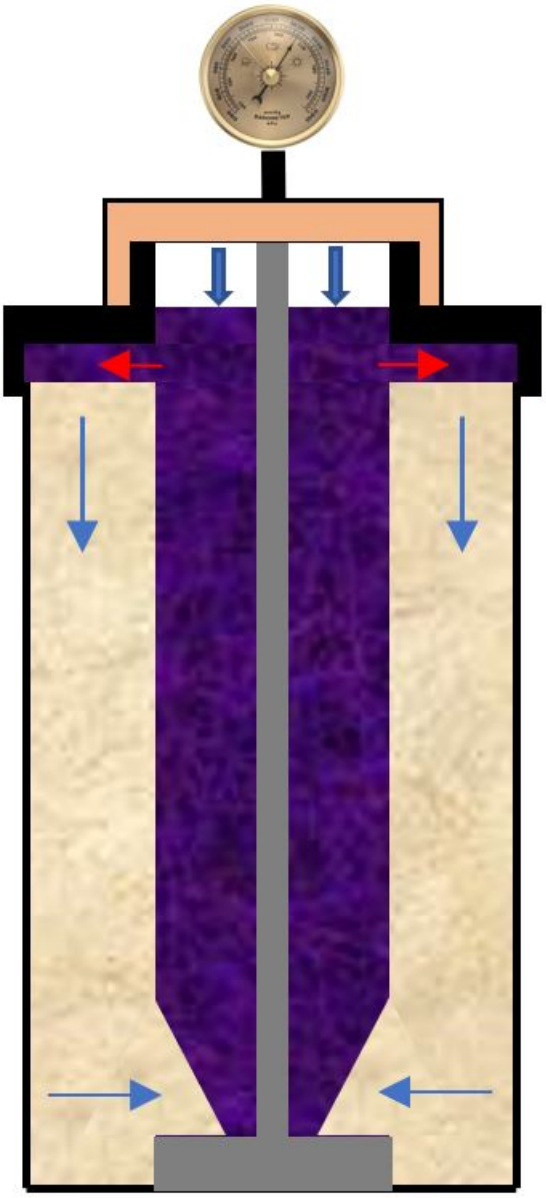

Figure 36: A sketch of a proposed suggestion about how the soil collapse could have occured. When the bentonite fluid was in between the soil and the cap, it could have formed a filter cake on which pressure would have been exerted by the bentonite fluid itself. in this case the fluid would have been able to flow out of the DPIA trough two tiny holes made on the top of the cap. The blue and red arrows represent the direction of the forces that incite the foil collapse.

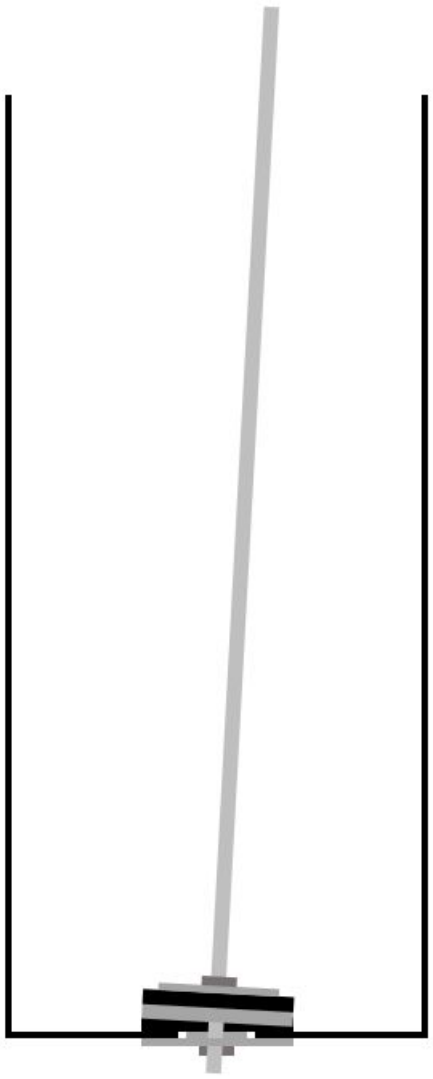

Figure 37: An exaggerated representation of how the axis of the pull out thread could deviate from the axis of the drill grout column.

7.2 Recommendations

The best part about the DPIA is that it can be used to test the friction between any two cylindrical materials, so that the friction between any arbitrary material could be measured. At first, the plan was to do the tests with PE, sand, clay and drill grout, but due to the construction time of the DPIA and the time needed to create the samples, it was decided that this was out of the scope of this thesis. When anyone decides to continue this research, the following is recommended.

The PVC screwing mechanism for attaching and removing different parts during the tests was not suited for sand. For example, when the cap of the DPIA had to be attached after filling the outer column with sand, particles would get stuck in between the cap (figure 15a) and screwing mechanism (figure 15g). Later, it was very hard to remove the cap so that it could be replaced with the pull out cap (figure 15h). Also, there had to be as little space in between the soil and the cap as possible to prevent the situation visualised in figure 36. But when the outer column was filled with too much sand. the cap could not be screwed all the way down onto the outer column. This caused the cap to be not water tight. Because of this, the bentonite fluid would flow out of the screwing mechanism of the cap. This way, the flow path of the bentonite fluid would not be trough the soil which would cause the sample to be useless. What made it even worse is that this was only noticed while pressuring the fluid, so the sample making process had to be redone entirely. It was tried to mark a certain height until where the column would have to be filled with soil, but this was not accurate enough. Also, water tight tape (teflon tape) was tried. This helped a lot, but it did not create a perfect water tight sealant. A solution that guarantees a water tight sealing while leaving no space in between the cap and the soil was not found. This is why it is suggested to use a cap that can be fixated with straps instead of a screwing mechanism. This way the lids can be removed with the least disturbance and it should leave a margin of error regarding the height of the soil in the outer column. This margin of error is created since the soil and the bottom of the cap can both be made to be a little bit compressible so that they are pressed onto each other which could make a water tight sealing.
Because of the fact that fluid flowed out of all kinds of pores in the DPIA, the total amount of fluid loss could not be measured. If this information is valuable for your research it is recommended to pay attention to this and try to make the DPIA totally water tight.

Appendix

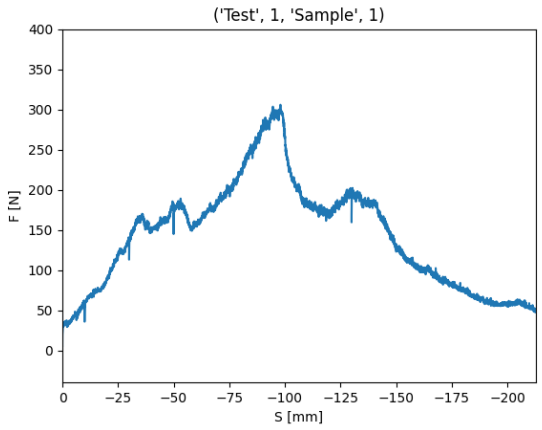

(a) Plotted results from test 1 sample 1

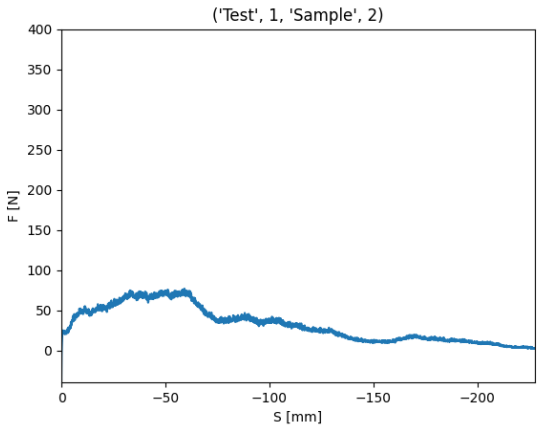

(b) Plotted results from test 1 sample 2

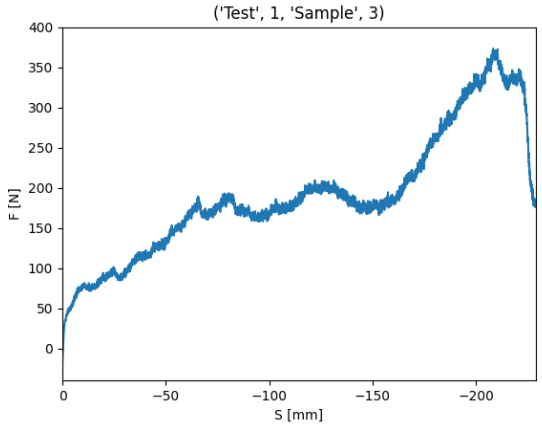

(c) Plotted results from test 1 sample 3

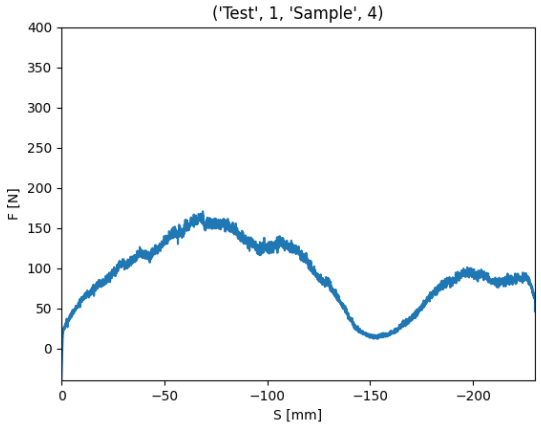

(d) Plotted results from test 1 sample 4

Figure 38: Plotted results from test 1

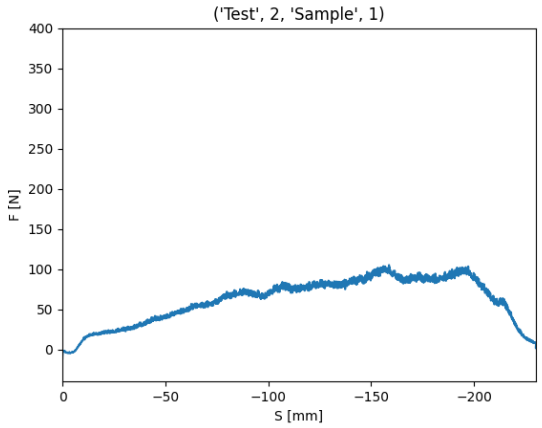

(a) Plotted results from test 2 sample 1

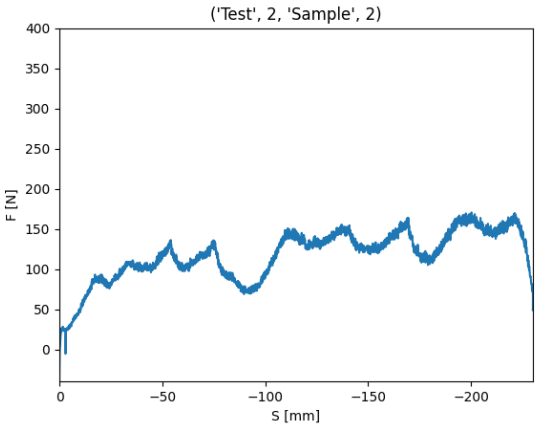

(b) Plotted results from test 2 sample 2

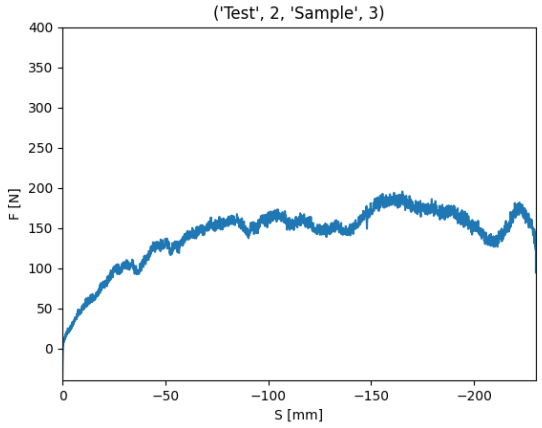

(c) Plotted results from test 2 sample 3

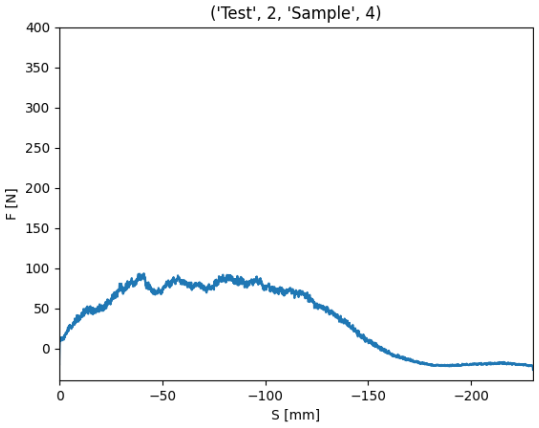

(d) Plotted results from test 2 sample 4

Figure 39: Plotted results from test 2

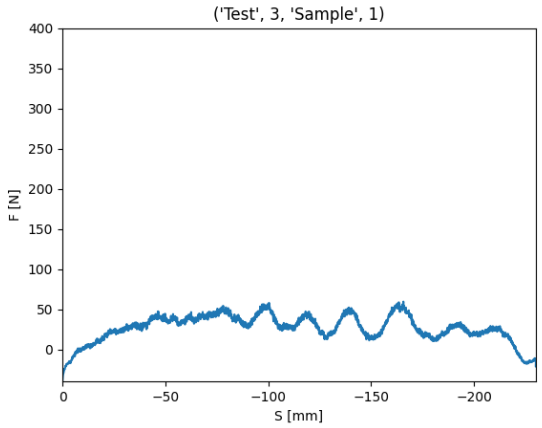

(a) Plotted results from test 3 sample 1

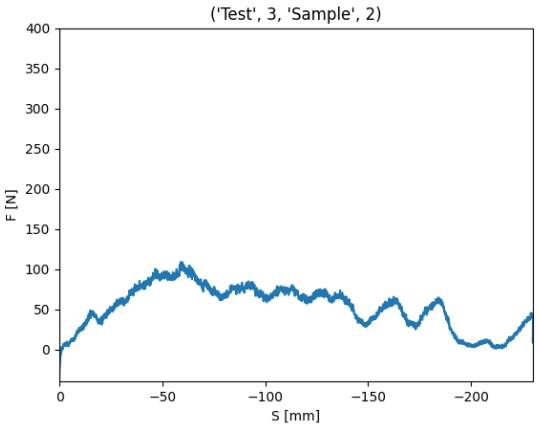

(b) Plotted results from test 3 sample 2

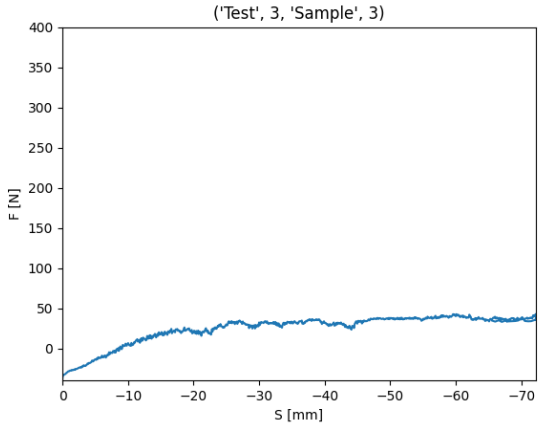

(c) Plotted results from test 3 sample 3

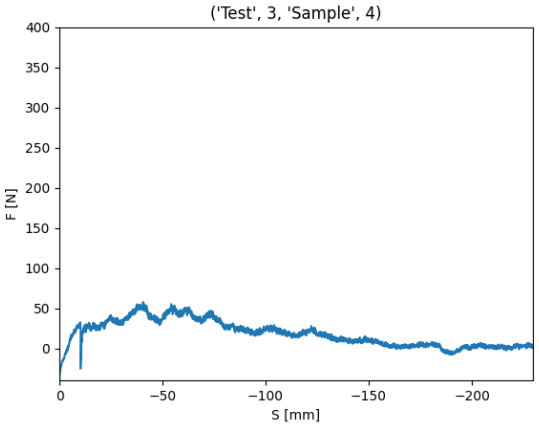

(d) Plotted results from test 3 sample 4

Figure 40: Plotted results from test 3

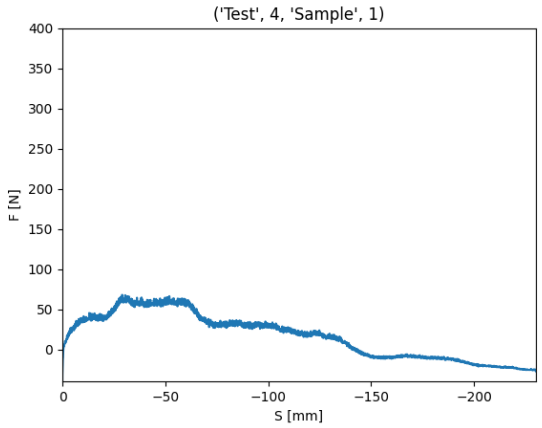

(a) Plotted results from test 4 sample 1

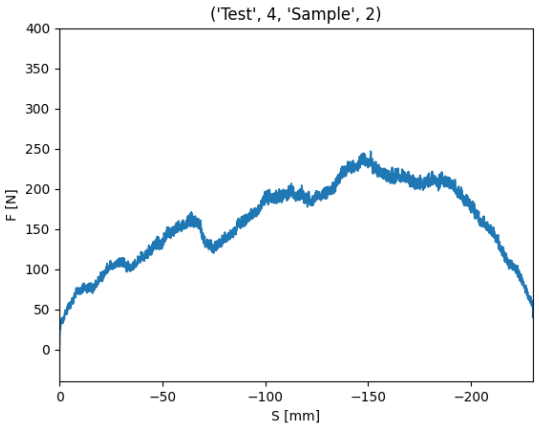

(b) Plotted results from test 4 sample 2

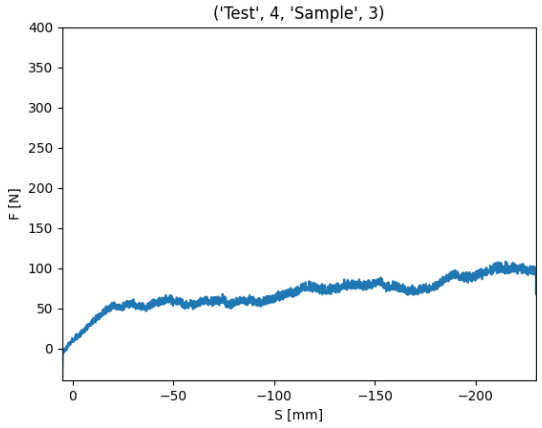

(c) Plotted results from test 4 sample 3

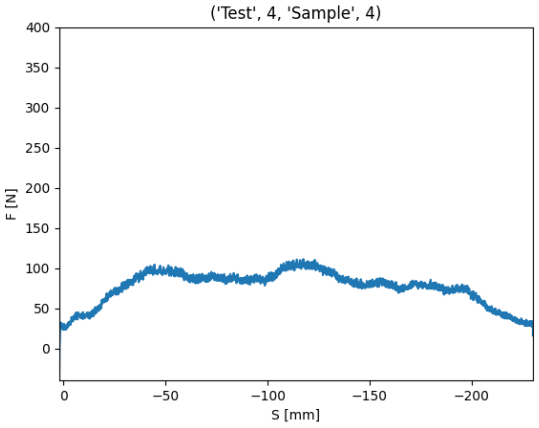

(d) Plotted results from test 4 sample 4

Figure 41: Plotted results from test 4

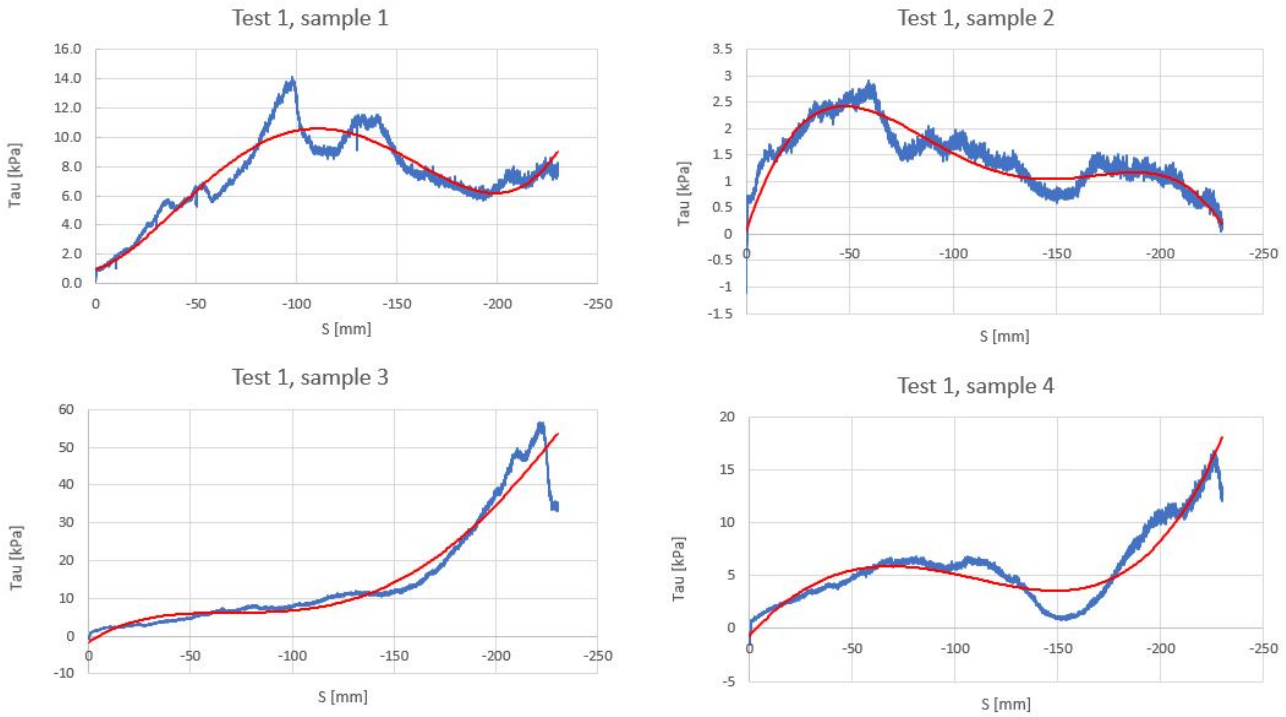

Figure 42: Normalisation of test 1

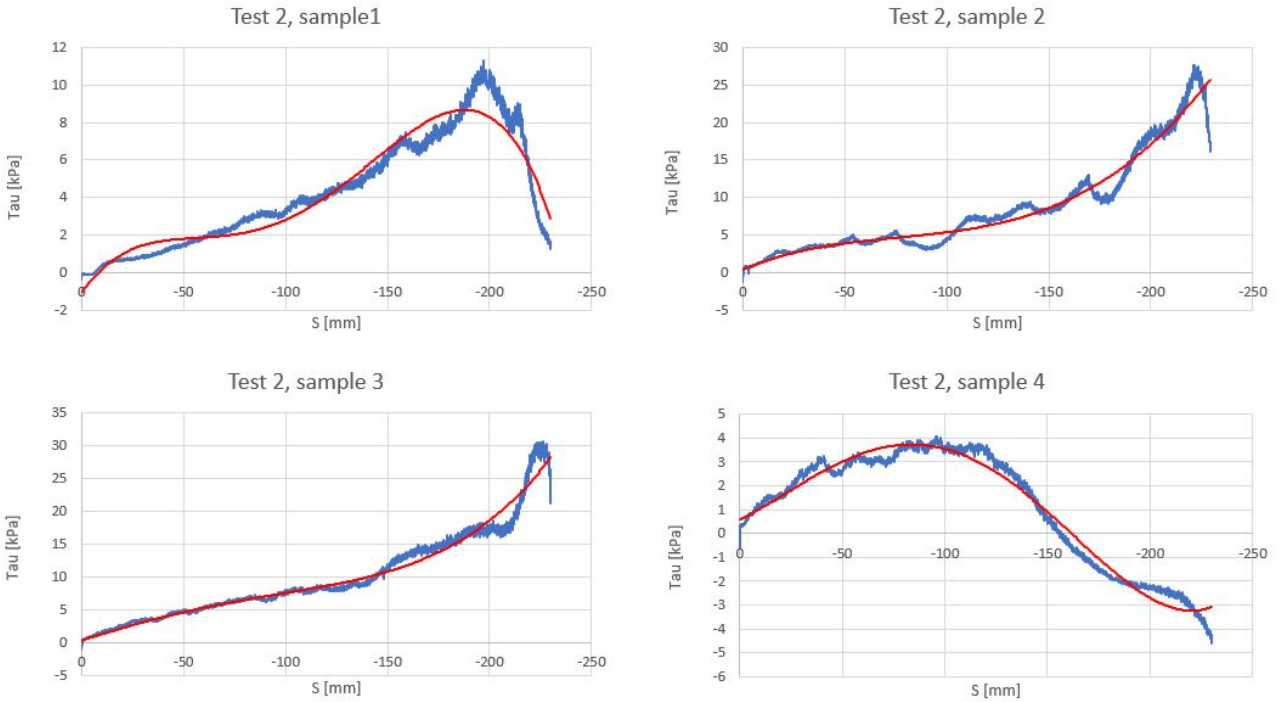

Figure 43: Normalisation of test 2

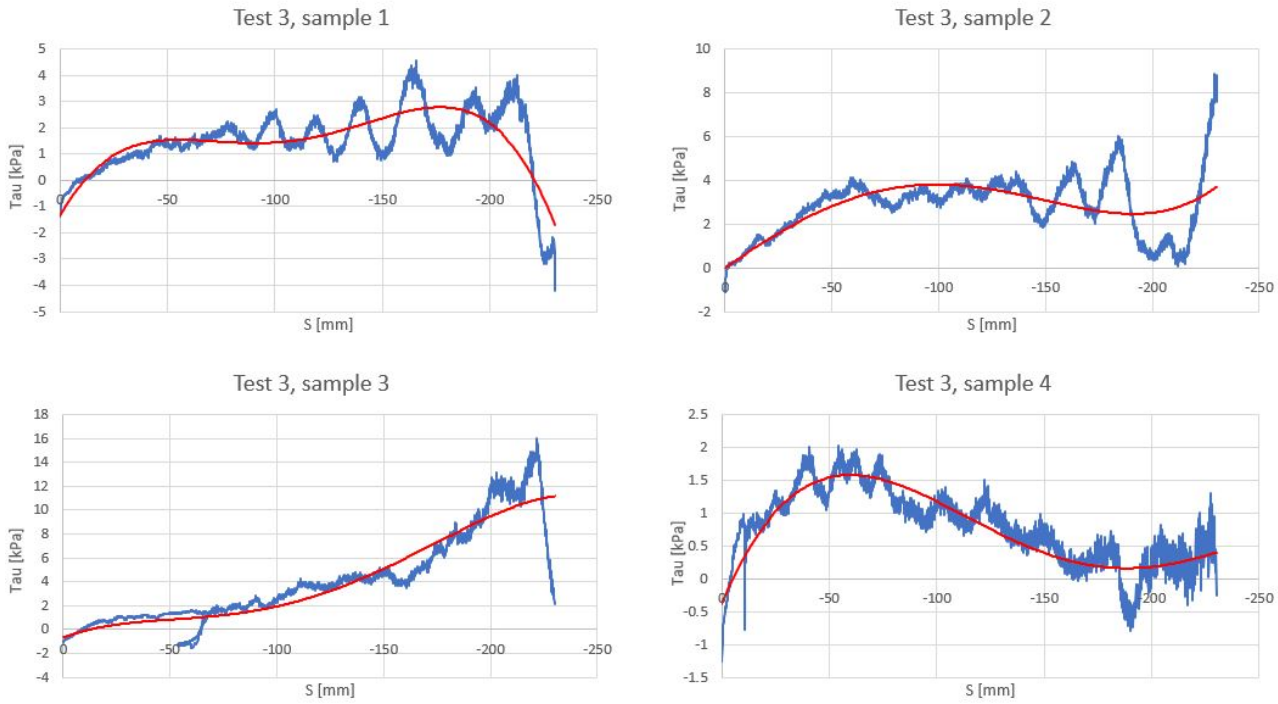

Figure 44: Normalisation of test 3

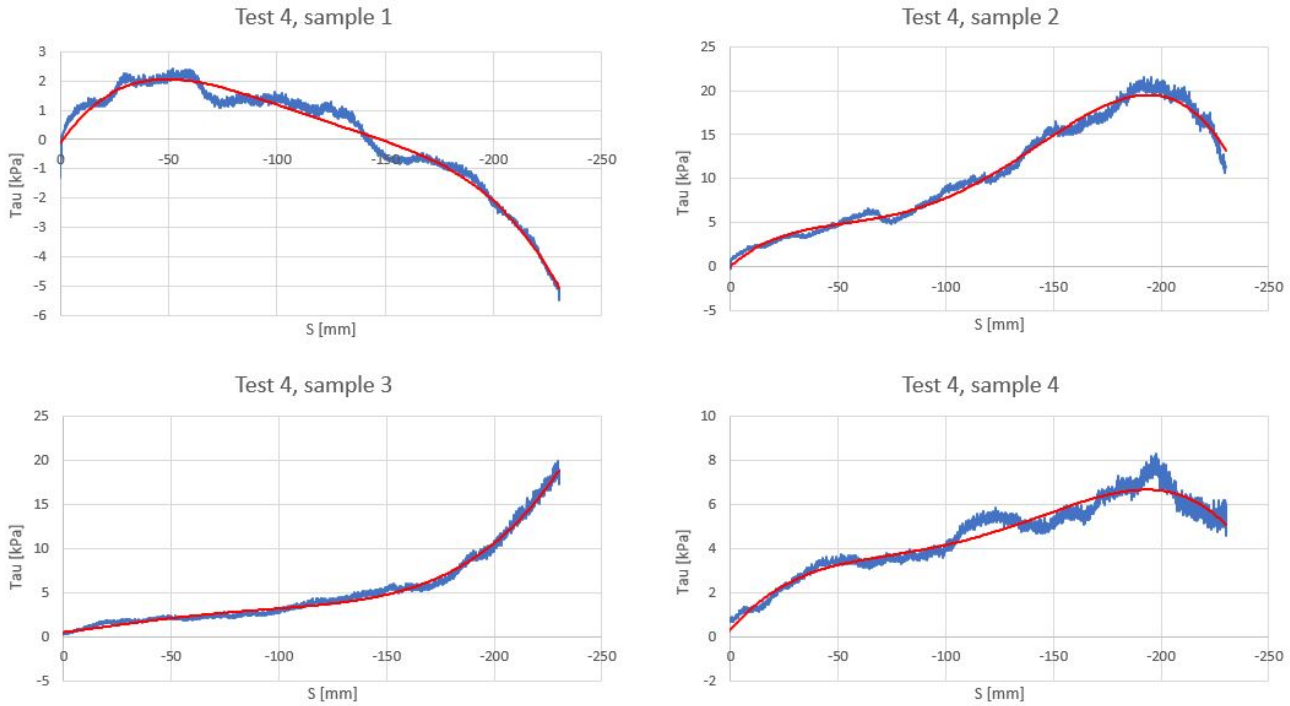

Figure 45: Normalisation of test 4

Test number	Sample number	Minimal pull out force [N]	Maximal pull out force [N]
1	1	138.4	187.0
1	2	0.0	29.6
1	3	230.0	278.7
1	4	61.6	110.2
4	1	0.0	19.0
4	2	133.0	181.6
4	3	9.9	58.5
4	4	8.2	56.9

Table 6: friction values. These were obtained by determining the maximum friction values from every test, thus the peak of every graph shown in Figure 8 and Figure 9.

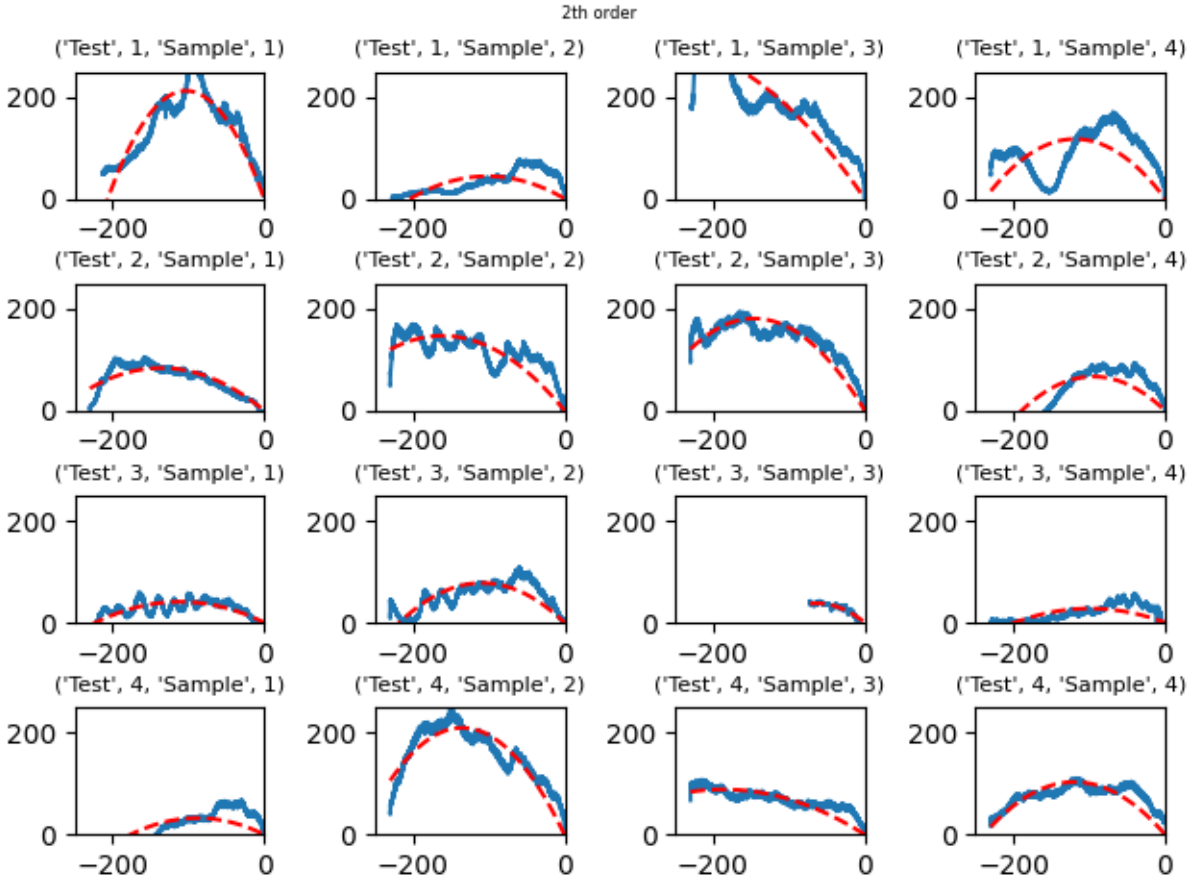

Figure 46: Second order polynomial fit

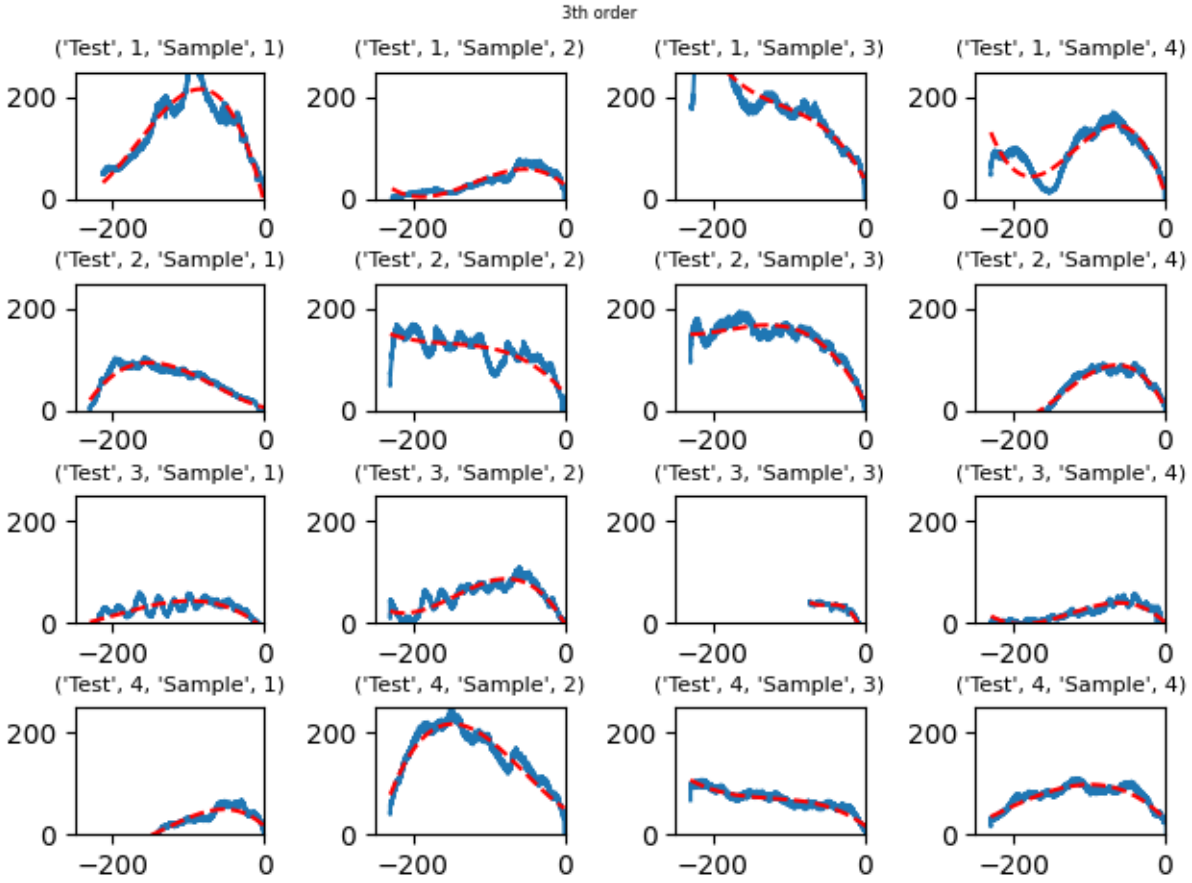

Figure 47: Third order polynomial fit

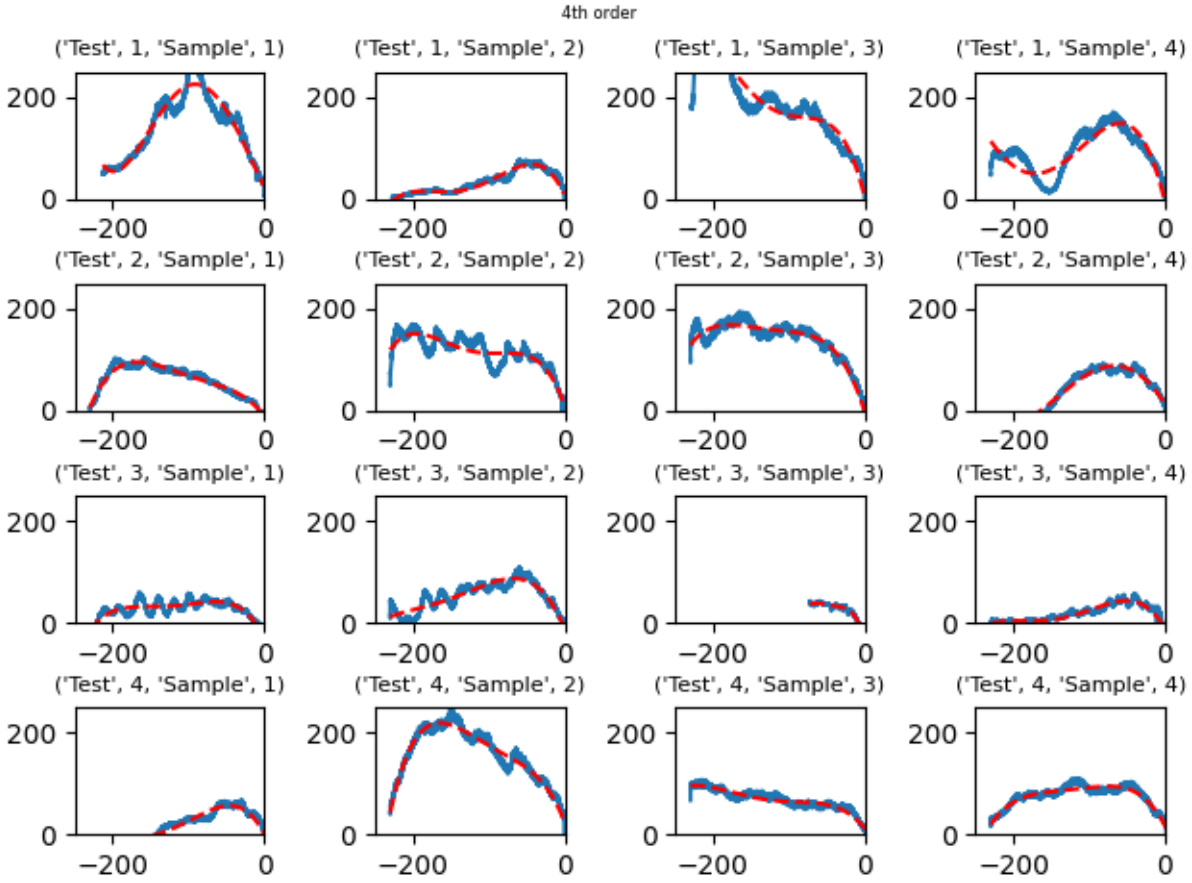

Figure 48: Fourth order polynomial fit

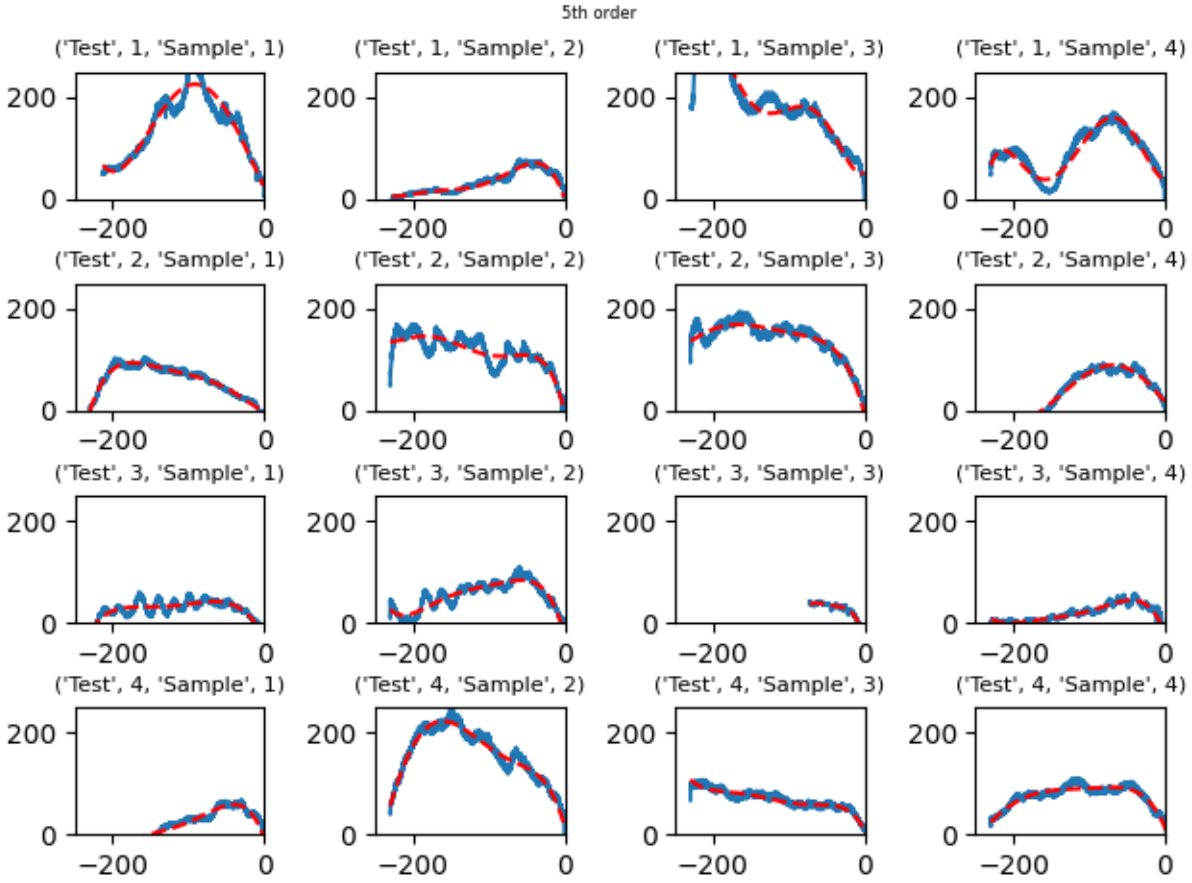

Figure 49: Fifth order polynomial fit

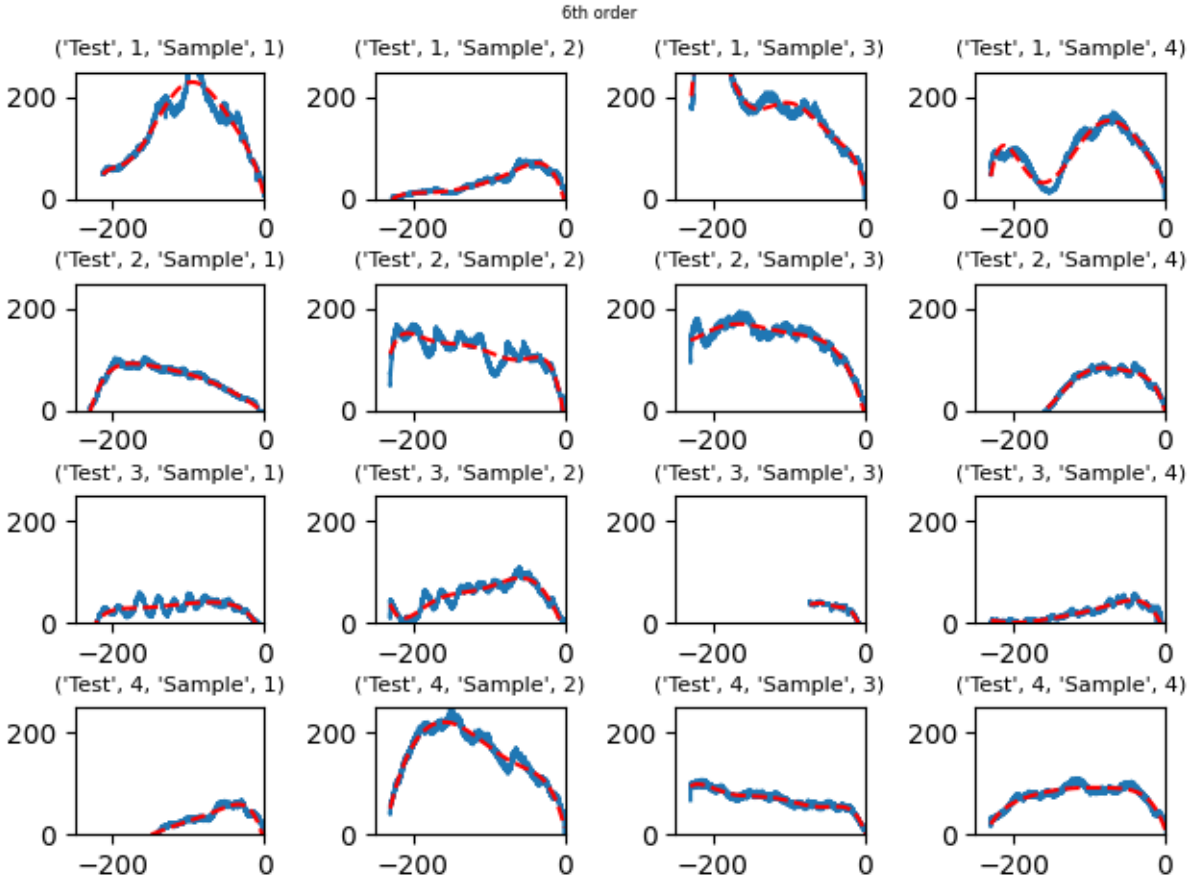

Figure 50: Sixth order polynomial fit

References

[1] G Appa Rao. "Performance Characteristics of Cement Grout in Precast Construction". In: 2019. DOI: 10.21012/fc10.233507.

[2] Barbara A. Plog et. al. "Strategies to Prevent Trenching-Related Injuries and Deaths". In: *The Center to Protect Workers' Rights* March (2006). URL: http://www.elcosh.org/record/document/1382/d000778.pdf.

[3] A. Barnes Barnes. "Thixotropy". In: *International Journal of Cosmetic Science* 70.1-2 (1997), pp. 1–33. ISSN: 14682494. DOI: 10.1111/j.1467-2494.1987.tb00472.x.

[4] Wouter Broere and A F van Tol. "Influence of Infiltration and Groundwater Flow on Tunnel Face Stability". In: *Geotechnical Aspects of Underground Construction in Soft Ground - 3rd International Symposium (IS-Tokyo)* (2000), pp. 339–344.

[5] Cebo Drill-grout. "Product Datablad Product Datablad Cebo Drill-Grout". In: 31.0 (1976), pp. 0–1.

[6] R W S Infromatie. "Colofon / metadata standaard". In: (2019).

[7] Sarvaiya Jayrajsinh et al. "Montmorillonite nanoclay as a multifaceted drug-delivery carrier: A review". In: *Journal of Drug Delivery Science and Technology* 39 (2017), pp. 200–209. ISSN: 17732247. DOI: 10.1016/j.jddst.2017.03.023. URL: http://dx.doi.org/10.1016/j.jddst.2017.03.023.

[8] M Kilchert and J Karstedt. "Schlitzwande als Trag-und Dichtungwande, Band 2, Standsicherheitberechnung von Schlitzwanden". In: *DIN, Berlin* Band 2 (1984), pp. 28–34.

[9] Shenghua Lv et al. "Use of graphene oxide nanosheets to regulate the microstructure of hardened cement paste to increase its strength and toughness". In: *CrystEngComm* 16.36 (Sept. 2014), pp. 8508–8516. ISSN: 14668033. DOI: 10.1039/c4ce00684d. URL: https://pubs.rsc.org/en/content/articlehtml/2014/ce/c4ce00684d%20https://pubs.rsc.org/en/content/articlelanding/2014/ce/c4ce00684d.

[10] A. Martinez and J. D. Frost. "The influence of surface roughness form on the strength of sand–structure interfaces". In: *Géotechnique Letters* 7.1 (2017), pp. 104–111. DOI: 10.1680/jgele.16.00169.

[11] P. Erik Mikkelsen. "Cement-bentonite grout backfill for borehole instruments". In: *Geotechnical News* 20.4 (2002), pp. 38–42. ISSN: 07100477.

[12] Fanlu Min, Wei Zhu, and Xiaorui Han. "Filter cake formation for slurry shield tunneling in highly permeable sand". In: *Tunnelling and Underground Space Technology* 38 (2013), pp. 423–430. ISSN: 08867798. DOI: 10.1016/j.tust.2013.07.024. URL: http://dx.doi.org/10.1016/j.tust.2013.07.024.

[13] H Muller-Kirchenbauer. *Stability of slurry trenches in inhomogeneous subsoil*. 1977, pp. 125–132.

[14] Vervangt Nen. "Nen 3650-1:2020". In: (2020).

[15] H Ostermayer and Foundation Engineering. "RESEARCH ON GROUND ANCHORS IN NON-COHESIVE SOILS Etude de tirants scellés dans des sols, pulvérulènts by". In: (), pp. 8–13.

[16] *Preinsulated bonded pipe systems for underground hot water networks*. 1995.

[17] Rebeca N. Sacramento et al. "Deep bed and cake filtration of two-size particle suspension in porous media". In: *Journal of Petroleum Science and Engineering* 126 (2015), pp. 201–210. ISSN: 09204105. DOI: 10.1016/j.petrol.2014.12.001. URL: http://dx.doi.org/10.1016/j.petrol.2014.12.001.

[18] M. Segad et al. "Ca/Na montmorillonite: Structure, forces and swelling properties". In: *Langmuir* 26.8 (2010), pp. 5782–5790. ISSN: 07437463. DOI: 10.1021/la9036293.

[19] Beatrix Kerkhoff Steven H. Kosmatka and William C. Panarese. *Design and Control Design and Control of*. 2008, p. 32. ISBN: 0893122173.

[20] Pinghe Sun et al. "Laboratory study of fluid properties owing to cutting intrusions during horizontal directional drilling". In: *Underground Space (China)* 5.1 (2020), pp. 20–29. ISSN: 24679674. DOI: 10.1016/j.undsp.2018.09.004. URL: https://doi.org/10.1016/j.undsp.2018.09.004.

[21] Andrew R. Tognon, R. Kerry Rowe, and Richard W.I. Brachman. "Evaluation of side wall friction for a buried pipe testing facility". In: *Geotextiles and Geomembranes* 17.4 (Aug. 1999), pp. 193–212. ISSN: 0266-1144. DOI: 10.1016/S0266-1144(99)00004-7.

[22] A. Verruijt. *Soil Mechanics*. 2001, p. 340. ISBN: 9780123693969. DOI: 10.1016/B0-12-369396-9/00228-8.

[23] X. Wang and R. L. Sterling. "Stability analysis of a borehole wall during horizontal directional drilling". In: *Tunnelling and Underground Space Technology* 22.5-6 (2007), pp. 620–632. ISSN: 08867798. DOI: 10.1016/j.tust.2007.01.002.

[24] WeijersWaalwijk. *Technische documentatie*. Tech. rep. 0. 2010, pp. 1–89.

[25] Xuefeng Yan et al. "Analysis of formation fracturing for the Maxi-HDD Qin River crossing project in China". In: *Tunnelling and Underground Space Technology* 53 (2016), pp. 1–12. ISSN: 08867798. DOI: 10.1016/j.tust.2015.11.018. URL: http://dx.doi.org/10.1016/j.tust.2015.11.018.

[26] Xufeng Yan et al. "Horizontal directional drilling: State-of-the-art review of theory and applications". In: *Tunnelling and Underground Space Technology* 72.June 2017 (2018), pp. 162–173. ISSN: 08867798. DOI: 10.1016/j.tust.2017.10.005. URL: https://doi.org/10.1016/j.tust.2017.10.005.

[27] Tong Yin et al. "Tunnelling and Underground Space Technology incorporating Trenchless Technology Research On the morphology and pressure-filtration characteristics of filter cake formation : Insight from coupled CFD – DEM simulations". In: 111.January 2020 (2021).